Chapter 2.3
Platforms with Multi-directional Total Thrust

Antonio Franchi

Abstract The chapter provides an overview of the basic modeling and the intrinsic properties of aerial platforms with multi-directional total thrust ability. When also fully-actuated, such platforms can modify the total wrench in body frame in any direction, thus allowing the control of position and orientation independently. Therefore, they are best suited for dexterous tasks, physical interaction, and for carrying aerial manipulators, because they do not suffer from the underactuation of standard collinear multirotors. The chapter includes a rigorous classification, a discussion on the possible input coupling, and on the capabilities and pitfalls of inverse-dynamics control approach for such platforms.

1 Introduction and Benefits of Multi-directional Total Thrust

Aerial vehicles have been thoroughly studied and applied in several fields and for several tasks, from simple remote sensing to the more challenging physical interaction with the environment and humans. The latter have been firstly targeted using aerial vehicles actuated by *multiple collinear rotors* and endowed with cables [289, 84, 291] rigid tools [207, 315] or a more complex robotic arm with a few degrees of freedom (DoFs) [88, 200, 292]. Collinear-rotor vehicles are energy efficient but underactuated because of the unidirectionality of the total thrust in the body frame. As a consequence the vehicle orientation is coupled with its translational motion, and the vehicle cannot *instantaneously* react to forces with any direction.

Cases in which a tool is rigidly fixed to the airframe have been presented in [101, 15, 317, 207, 100]. The impossibility of controlling the 6D (position plus orientation) dynamics of the end-effector limits the potential use cases and also creates stability issues. In fact, it has been shown that in the presence of interactions with points of the airframe other than the vehicle center of mass (CoM) the internal dynamics of underactuated multirotors is not guaranteed to be stable, and it is, in general, neither easy to stabilize nor practical for real applications [207].

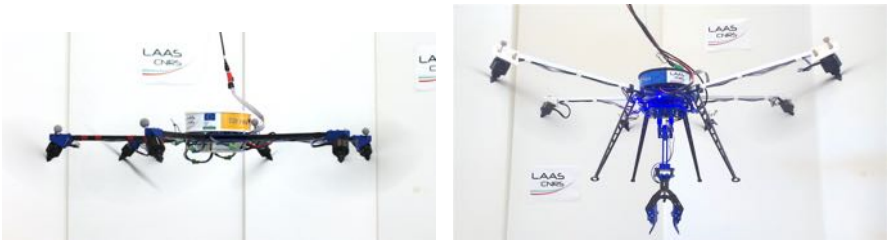

Fig. 38 The TiltHex (left) and the OTHex (right): two fully actuated hexarotors by LAAS-CNRS. They are capable of 6D motion (fully-decoupled pose) and 6D physical interaction thanks to the non-collinear orientations of the thrust forces produced by its propellers and the use of suitable physical interfaces, such as the passive gripper of the OTHex, optimized for bar lifting.

To overcome such limitation, the main approach has been to attach an n-DoF robotic arm to the aerial platform [200, 199, 18, 138, 292], a solution which aims at overcoming the underactuation of the end-effector dynamics exploiting the increased number of actuators provided by the arm. In this way, a fully actuated 6D force control at the end-effector side becomes possible [313]. However, this solution comes with a few drawbacks as well, the main being that: *i)* a robotic arm strongly decreases the payload and flight time due to its own weight; *ii)* the system is much more complex from a mechanical point of view than a single airframe with a rigid tool and, thus, it is more expensive to build and also requires more maintenance and repairing costs across its operational life; *iii)* lateral forces in body frame, which cannot be provided by the aerial platform itself, have to be generated through the dynamical/inertial coupling between the arm and the aerial robot: the proper mastering of the dynamical coupling is something that has to be necessarily exploited in order to get the sought benefits in terms of 6D force control. This, in turn, requires the knowledge of the precise dynamical model and a very accurate measurement of the system inputs and states (position, orientation, linear and angular velocities). As a matter of fact, these requirements are extremely hard to achieve in real world conditions (especially the former). For this reason, kinematic-only approaches have been preferred for real world validations, see e.g., [200, 199], at the expense of losing the main benefits for which the manipulator was introduced.

Summarizing, standard flying platforms are underactuated and, thus, incapable of 6D end-effector force control. On the other side, to bring a full manipulator up to the air to perform the sought 6D end-effector force control is often excessively complex and may introduce more problems than benefits, depending on the task. To solve all these problems at once and finally achieve the sought full 6D force control of the aerial interaction, is instead enough to let the aerial vehicle possess the minimal requirements to perform such interaction with a rigidly attached end-effector. Such requirements can be satisfied with the use of a multirotor with *generically-oriented fixed propellers* (GOFP) instead of the more common *collinearly-oriented fixed propeller* (COFP) architectures [254]. In GOFP platforms, which appeared in the robotics literature only recently (see, e.g., [237, 306, 244, 41, 225]), the full-actuation is achieved by a more general propeller position and orientation. The dif-

ference between the underactuated platform and the last approach is that, in the former approach, all the propellers have the same orientation while, in the second approach, every propeller orientation is different. The latter approach is, thus, able to control independently the translational and angular acceleration in contact-free flight, or any of the six components of the exerted wrench when in contact, thus allowing full and dexterous 6D force control, which makes them much more suited for physical interaction tasks than standard COFP platforms. An example of a fully actuated GOFP platform is the OTHex by LAAS-CNRS, depicted in Figure 38. This platform has six propellers with coplanar centers and non-collinear directions of rotation, a configuration which makes it possible the 6D physical interaction and manipulation [280].

Another solution to obtain full-actuation consists of actively tilting the whole propeller groups [254, 255, 170], a solution which is called thrust vectoring or tilting propeller. This solution however is subject to the same drawbacks of the solutions employing a manipulator arm, since they require extra actuation, mechanical complexity, and weight. Furthermore, they cannot in general guarantee instantaneous disturbance rejection or fast force exertion since the propellers might have to be re-oriented, which again takes some non-negligible time.

In this Chapter we introduce a basic but effective model of GOFP platforms and provide a major classification and properties of such vehicles. In particular, the model of the total thrust and moment generation, and classification with respect to actuation singularity are provided in Sec. 2. In Sec. 3 we describe the capability of producing a multi- or omnidirectional total thrust when employing propellers with uni-directional lift force. The possible coupling between total thrust and total moment is described in Sec. 4. Sec. 5 introduces the inverse dynamics control strategy for fully actuated platforms and highlights its limits, which will be overcome in Chapter 3.6. Finally, conclusions are drawn in Sec. 6.

2 Platforms with Generically-Oriented Fixed Propellers

Let us define an inertial world frame $\mathscr{F}_W = \{O_W, \mathbf{x}_W, \mathbf{y}_W, \mathbf{z}_W\}$ where O_W is its origin, placed arbitrarily, and $(\mathbf{x}_W, \mathbf{y}_W, \mathbf{z}_W)$ are the orthogonal unit vectors. We consider $\mathbf{z}_W$ parallel and opposite to the gravity vector. Then we define the body frame $\mathscr{F}_B = \{O_B, \mathbf{x}_B, \mathbf{y}_B, \mathbf{z}_B\}$ rigidly attached to the vehicle and centered in O_B, the vehicle center of mass (CoM). The position of O_B and orientation of $\mathscr{F}_B$ w.r.t. $\mathscr{F}_W$ are described by the vector $\mathbf{p}_b \in \mathbb{R}^3$ and the rotation matrix $\mathbf{R}_b \in SO(3)$, respectively. Then we define by the vector $\mathbf{v}_b \in \mathbb{R}^3$ the translational velocity of O_B expressed in $\mathscr{F}_W$, and by $\boldsymbol{\omega}_b^b \in \mathbb{R}^3$ the angular velocity of $\mathscr{F}_B$ w.r.t. $\mathscr{F}_W$ and expressed in $\mathscr{F}_B$. The generic vehicle, with only 3 of the n propellers, is depicted in Fig. 112.

The vehicle is modeled as a rigid body with mass $m \in \mathbb{R}_{>0}$ and moment of inertia about O_B, defined w.r.t. $\mathscr{F}_B$, described by the positive definite matrix $\mathbf{I}_b \in \mathbb{R}^{3\times3}$. The dynamics of the system is computed applying the Newton-Euler equations, thus obtaining $\dot{\mathbf{p}}_b = \mathbf{v}_b$, $\dot{\mathbf{R}}_b = \mathbf{R}_b \Omega_b$, and

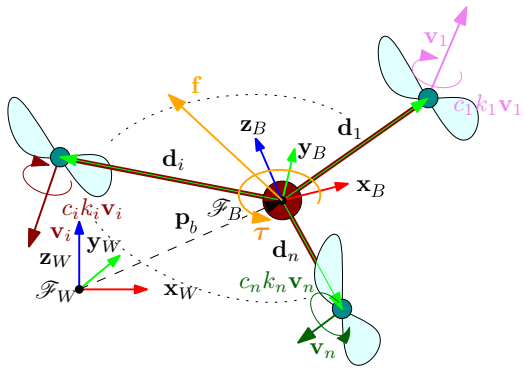

Fig. 39 Schematic representation of a multirotor with generically oriented fixed propellers and its main quantites. Only three of the n propellers are shown.

$$\underbrace{\begin{bmatrix} m\mathbf{I}_3 & \mathbf{0} \\ \mathbf{0} & \mathbf{I}_b \end{bmatrix}}_{\mathbf{M}_R} \underbrace{\begin{bmatrix} \dot{\mathbf{v}}_b \\ \dot{\boldsymbol{\omega}}_b^b \end{bmatrix}}_{\mathbf{a}} = \underbrace{\begin{bmatrix} -g\mathbf{e}_3 \\ -\mathbf{I}_b \boldsymbol{\omega}_b^b \times \boldsymbol{\omega}_b^b \end{bmatrix}}_{\mathbf{b}_R} + \underbrace{\begin{bmatrix} \mathbf{R}_b & \mathbf{0} \\ \mathbf{0} & \mathbf{I}_3 \end{bmatrix}}_{\mathbf{G}_R} \begin{bmatrix} \mathbf{f}_u^b \\ \boldsymbol{\tau}_u^b \end{bmatrix}, \tag{40}$$

where $\mathbf{e}_3 = [0\ 0\ 1]^\top$, $\Omega_b = \mathbf{S}(\boldsymbol{\omega}_b^b)$ is the skew symmetric matrix relative to $\boldsymbol{\omega}_b^b$, $\mathbf{f}_u^b \in \mathbb{R}^3$ and $\boldsymbol{\tau}_u^b \in \mathbb{R}^3$ are the controllable total input force and torque expressed in $\mathscr{F}_B$, respectively.

Considering a multirotor with n rotors, each of them produces a lift force and a moment due to the drag force [299]. All together they generate the total force (or thrust) and moment, $\mathbf{f}$ and $\boldsymbol{\tau}$, respectively,[1] expressed as:

$$\mathbf{w} = \left[\mathbf{f}^\top \boldsymbol{\tau}^\top\right]^\top = \left[\mathbf{G}_1^\top \mathbf{G}_2^\top\right]^\top \left[u_1 \ \dots \ u_n\right]^\top = \mathbf{G}\mathbf{u}. \tag{41}$$

The matrixes $\mathbf{G} \in \mathbb{R}^{6\times n}$, $\mathbf{G}_1 \in \mathbb{R}^{3\times n}$, and $\mathbf{G}_2 \in \mathbb{R}^{3\times n}$ are called the *full allocation matrix*, the *force allocation matrix* and the *moment allocation matrix*, respectively. The control $u_i \in \mathbb{R}$ is typically equal to $\omega_i|\omega_i|$, where $\omega_i \in \mathbb{R}$ is the i-th propeller rotational speed. $\mathbf{G}_1$ and $\mathbf{G}_2$ have the following structure

$$\mathbf{G}_1 = \left[\mathbf{v}_1 \ \cdots \ \mathbf{v}_n\right], \tag{42}$$

$$\mathbf{G}_2 = \left[\mathbf{d}_1 \times \mathbf{v}_1 \ \cdots \ \mathbf{d}_n \times \mathbf{v}_n\right] + \left[c_1 k_1 \mathbf{v}_1 \ \cdots \ c_n k_n \mathbf{v}_n\right], \tag{43}$$

where i) $\mathbf{v}_i \in \mathbb{R}^3$ are the coordinates, in $\mathscr{F}_B$, of the lift force generated by the i-th propeller when $u_i = 1$. In this formulation the aerodynamic coefficient that maps propeller speed into thrust intensity, typically called lift factor c_T, is $c_{Ti} = \|\mathbf{v}_i\| = v_i$; ii) $\mathbf{d}_i$ is the position of the center of the i-th propeller in body frame; iii) $c_i = -1$ ($c_i = 1$) if the i-th propeller angular velocity vector has the same direction of $\mathbf{v}_i$ ($-\mathbf{v}_i$) when $u_i > 0$, i.e., the propeller spins CCW (CW) when watched from its top;

[1] In the following we omit the subscripts and superscripts when there is no risk of confusion.

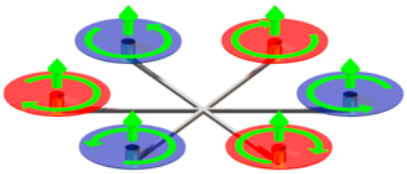

Fig. 40 A standard underactuated collinear hexarotor.

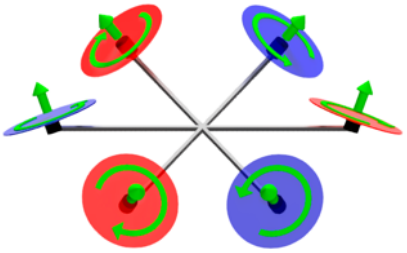

Fig. 41 The fully actuated non-collinear hexarotor called 'TiltHex', by LAAS-CNRS.

iv) $k_i \in \mathbb{R}$ is the constant ratio between the i-th propeller lift force and the drag moment, typically denoted with c_Q/c_T in the literature. The following is a well known and easy-to-prove fact.

Fact 1 (translation invariance) $\mathbf{G}$ *does not change if* $\mathbf{d}_i$ *is replaced with* $\mathbf{d}_i + \lambda_i \mathbf{v}_i$ *for any* $i = 1, \dots, n$ *and* $\lambda_1, \dots, \lambda_n \in \mathbb{R}$.

We introduce now the basic concept of multirotor design. Let us first define $\mathbf{c} = [c_1 \cdots c_n]^\top$ and $\mathbf{k} = [k_1 \cdots k_n]^\top$.

Definition 1 *A multirotor* design *is a tuple* $\mathscr{D} = (n, \mathbf{c}, \mathbf{k}, \mathbf{d}_1, \dots, \mathbf{d}_n, \mathbf{v}_1, \dots, \mathbf{v}_n)$, *which describes the number of propellers n, their aerodynamic characteristics, locations and orientations w.r.t.* $\mathscr{F}_B$. *We call the tuples* $(\mathbf{v}_1, \dots, \mathbf{v}_n)$ *and* $(n, \mathbf{c}, \mathbf{k}, \mathbf{d}_1, \dots, \mathbf{d}_n)$ *the* vectoring part *and the* etero-vectoring part *of* $\mathscr{D}$, *respectively.*

A first important classification of multirotor design is the following

Definition 2 *A multirotor design is:*

- *Underactuated if rank* $(\mathbf{G}) < 6$
- *Fully actuated if rank* $(\mathbf{G}) = 6$

furthermore, the multirotor translational (resp. rotational) dynamics are

- *Underactuated if rank* $(\mathbf{G}_1) < 3$ *(resp. rank* $(\mathbf{G}_2) < 3$*)*
- *Fully actuated if rank* $(\mathbf{G}_1) = 3$ *(resp. rank* $(\mathbf{G}_2) = 3$*).*

Full actuation requires $n \geq 6$, which is however, only a necessary condition. In fact, classical multirotor designs, like the one depicted in Fig. 40 have the $\mathbf{v}_1, \dots, \mathbf{v}_n$ all aligned and therefore rank $(\mathbf{G}_1) = 1$, which means that their translational dynamics is underactuated. On the other hand they are such that rank $(\mathbf{G}_2) = 3$, i.e., the rotational dynamics is fully actuated, and rank $(\mathbf{G}) = 4$. Other designs, such as the one depicted in Fig. 41, named TiltHex, by LAAS-CNRS, and presented in [237], has the $\mathbf{v}_1, \dots, \mathbf{v}_n$ non collinear and such that rank $(\mathbf{G}) = 6$ which makes it a fully actuated platform.

Notice that choosing non-collinear $\mathbf{v}_i$'s is a necessary but non-sufficient condition to obtain full actuation, in fact one has to ensure that all the 6 row vectors of $\mathbf{G}$ are linearly independent.

3 Multi-directional and Omnidirectional Total Thrust Platforms

We denote with $\mathbf{1}$ the column vector with all ones. Its size is understood from the context. Given two vectors $\mathbf{x}$ and $\mathbf{y}$, the notations $\mathbf{x} \geq \mathbf{y}$, $\mathbf{x} > \mathbf{y}$ have to be intended component-wise. Accordingly, we define $\mathbb{R}^n_{\geq \mathbf{0}} = \{\mathbf{x} \in \mathbb{R}^n | \mathbf{x} \geq \mathbf{0}\}$ and $\mathbb{R}^n_{> \mathbf{0}} = \{\mathbf{x} \in \mathbb{R}^n | \mathbf{x} > \mathbf{0}\}$, called the non-negative orthant and the positive orthant of $\mathbb{R}^n$, respectively.

Propellers can be of mainly two types: mono-directional and bidirectional. Mono-directional thrusters are the cheapest and most common solution but can produce lift only in one direction, a constraint which can be encoded imposing $\mathbf{u} \in \mathbb{R}^n_{\geq \mathbf{0}}$ in (41). Bidirectional thrust rotors are able to invert the direction of the lift force by inverting either the motor rotation or the propeller angle of attack. However such rotors have several issues: i) scarceness of reversible Electronic Speed Controllers (ESC) for brushless motors, ii) lower energetic efficiency compared to unidirectional rotors, iii) lower controllability of the exerted force at low speeds, and iv) extra mechanical complexity and increased weight and thus energy consumption (in case of variable pitch propellers). Such propellers have the advantage that $\mathbf{u} \in \mathbb{R}^n$ in (41). Let us denote with U the set of admissible inputs: $U = \mathbb{R}^n_{\geq \mathbf{0}}$ for mono-directional thrusters and $U = \mathbb{R}^n$ for bidirectional propellers. Then let us define the set of attainable wrenches $W = \{\mathbf{w} \in \mathbb{R}^6 \,|\, \exists \mathbf{u} \in U \; s.t. \; \mathbf{w} = \mathbf{G}\mathbf{u}\}$, the set of attainable total thrusts $\Phi = \{\mathbf{f} \in \mathbb{R}^3 \,|\, \exists \mathbf{u} \in U \; s.t. \; \mathbf{w} = \mathbf{G}_1\mathbf{u}\}$, and the set of attainable total moments $\Theta = \{\boldsymbol{\tau} \in \mathbb{R}^3 \,|\, \exists \mathbf{u} \in U \; s.t. \; \mathbf{w} = \mathbf{G}_2\mathbf{u}\}$.

The following additional classification of multirotor design holds.

Definition 3 *A fully actuated multirotor design for which $\Theta = \mathbb{R}^3$ is a*

- multi-directional total thrust platform *if* $\Phi \subsetneq \mathbb{R}^3$
- omnidirectional total thrust platform *if* $\Phi = \mathbb{R}^3$.

A multi-directional thrust platform can produce a total force (independent from total moment) in multiple (but not all) directions. As a consequence it can hover with multiple (but not all) orientations. An omnidirectional thrust platform can produce a total force (independent from total moment) in any direction and can hover with any orientation. Omnidirectional platforms can be oriented in any direction and can compensate/exert any force independently, thus allowing applications that are impossible with other platforms, including safe human interaction, 360° aerial photography, etc. In [225] and [41] two omnidirectional total thrust vehicles are proposed with 6 and 8 tilted bidirectional thrust rotors, respectively. As explained before, bidirectional thrusters have several drawbacks. The authors in [290] thoroughly investigate *if and how* it is instead possible to obtain omnidirectional thrust vehicles with fixed and uni-directional thrusters, a solution that overcome all the problems of the aforementioned solutions using bidirectional propellers. One of the main results is summarized in the following:

Proposition 1 ([290]) *If $U = \mathbb{R}^n$ then a fully actuated multirotor is also omnidirectional. If $U = \mathbb{R}^n_{\geq \mathbf{0}}$ then a fully actuated multirotor is also omnidirectional if and only if*

$$null\,(\mathbf{G}) \cap \mathbb{R}^n_{>\mathbf{0}} \neq \emptyset, \tag{44}$$

otherwise, it is a multi-directional platform.

In other words, a fully-actuated platform with bidirectional propellers is also an omnidirectional total thrust platform. On the other side, a fully-actuated platform with mono-directional propellers is in general only a multi-directional total thrust platform. For such platforms, it is required that (44) holds too, which implies that $n \geq 7$. This latter is however only a necessary condition. In [290] the authors propose also a control allocation strategy and an algorithm for optimally design such platforms.

4 Coupling Between Total thrust and Total Moment

In the following we assume a fully-actuated rotational dynamics, i.e.,

$$\text{rank}\,(\mathbf{G}_2) = 3. \tag{45}$$

The input space $\mathbb{R}^n$ can always be partitioned in the orthogonal subspaces $\text{im}\left(\mathbf{G}_2^\top\right)$ and $\text{im}\left(\mathbf{G}_2^\top\right)^\perp = \text{null}\,(\mathbf{G}_2)$, such that the vector $\mathbf{u}$ can be rewritten as the sum of two terms, namely

$$\mathbf{u} = \mathbf{T}_2\tilde{\mathbf{u}} = [\mathbf{A}_2 \;\; \mathbf{B}_2] \begin{bmatrix} \tilde{\mathbf{u}}_A \\ \tilde{\mathbf{u}}_B \end{bmatrix} = \mathbf{A}_2\tilde{\mathbf{u}}_A + \mathbf{B}_2\tilde{\mathbf{u}}_B, \tag{46}$$

where $\mathbf{T}_2 = [\mathbf{A}_2\,\mathbf{B}_2] \in \mathbb{R}^{n\times n}$ is an orthogonal matrix such that $\text{im}(\mathbf{A}_2) = \text{im}(\mathbf{G}_2^\top)$ and $\text{im}(\mathbf{B}_2) = \text{null}\,(\mathbf{G}_2)$. Note that, because of (45), $\mathbf{A}_2 \in \mathbb{R}^{n\times 3}$ is full rank, i.e., $\text{rank}\,(\mathbf{A}_2) = 3$, while $\mathbf{B}_2 \in \mathbb{R}^{n\times n-3}$ has $\text{rank}\,(\mathbf{B}_2) = n-3$. Given this partition, we have

$$\boldsymbol{\tau} = \mathbf{G}_2\mathbf{T}_2\tilde{\mathbf{u}} = \mathbf{G}_2\mathbf{A}_2\tilde{\mathbf{u}}_A, \tag{47}$$

$$\mathbf{f} = \mathbf{G}_1\mathbf{T}_2\tilde{\mathbf{u}} = \mathbf{G}_1\mathbf{A}_2\tilde{\mathbf{u}}_A + \mathbf{G}_1\mathbf{B}_2\tilde{\mathbf{u}}_B =: \mathbf{f}^A + \mathbf{f}^B. \tag{48}$$

The matrix $\mathbf{G}_2\mathbf{A}_2$ in (47) is nonsingular thus any moment $\boldsymbol{\tau} \in \mathbb{R}^3$ can be virtually implemented by setting $\tilde{\mathbf{u}}_A = (\mathbf{G}_2\mathbf{A}_2)^{-1}\boldsymbol{\tau}$ in conjunction with any $\tilde{\mathbf{u}}_B \in \mathbb{R}^{n-3}$.

The control force, which obviously belongs to $\mathfrak{F} := \text{im}(\mathbf{G}_1)$, is split in two components: $\mathbf{f} = \mathbf{f}^A + \mathbf{f}^B$. The component $\mathbf{f}^A = \mathbf{G}_1\mathbf{A}_2\tilde{\mathbf{u}}_A$ represents the 'spurious' force generated by the allocation of the input needed to obtain a non-zero control moment. This component belongs to the subspace $\mathfrak{F}_A := \text{im}(\mathbf{G}_1\mathbf{A}_2) \subset \mathbb{R}^n$. The component $\mathbf{f}^B = \mathbf{G}_1\mathbf{B}_2\tilde{\mathbf{u}}_B$ instead represents a force that can be assigned independently from the control moment by allocating the input $\mathbf{u}$ in $\text{im}(\mathbf{B}_2) = \text{null}\,(\mathbf{G}_2)$. This 'free' force component belongs to the subspace $\mathfrak{F}_B := \text{im}(\mathbf{G}_1\mathbf{B}_2) \subset \mathbb{R}^n$ and it is obtained by assigning $\tilde{\mathbf{u}}_B$. Being $\mathbf{T}_2$ nonsingular, we have that $\mathfrak{F} = \mathfrak{F}_A + \mathfrak{F}_B$. It is instru-

		∃ decoupled direction		
			∃ decoupled plane	
	$\dim\mathfrak{F}_B=0$	$\dim\mathfrak{F}_B=1$	$\dim\mathfrak{F}_B=2$	$\dim\mathfrak{F}_B=3$
$\mathfrak{F}_B\subsetneq\mathfrak{F}$	FC	PC and SD1	PC and SD2	N/A
$\mathfrak{F}_B=\mathfrak{F}$	N/A	UC and SD1	UC and SD2	D3 (UC)
	$(\dim\mathfrak{F}\geq 1)$	$(\dim\mathfrak{F}\geq 1)$	$(\Rightarrow\dim\mathfrak{F}\geq 2)$	$(\Rightarrow\dim\mathfrak{F}=3)$

Table 9 A table recalling the fundamental properties of the actuation of a GOFP.

mental to recall that $1\leq\dim\mathfrak{F}\leq 3$ because $\text{rank}\,(\mathbf{G}_1)\geq 1$, and that $\mathfrak{F}_B\subseteq\mathfrak{F}$, thus $\dim\mathfrak{F}\geq\dim\mathfrak{F}_B$.

The dimension of $\mathfrak{F}_B$ and its relation with $\mathfrak{F}$ sheds light upon the platform actuation capabilities. The following two sets of definitions are devoted to this purpose.

Definition 1. A platform with generically-oriented fixed propellers (GOFP) is

- *fully coupled* (FC) if $\dim\mathfrak{F}_B=0$ (i.e., if $\mathbf{G}_1\mathbf{B}_2=\mathbf{0}$)
- *partially coupled* (PC) if $\dim\mathfrak{F}_B\in\{1,2\}$ and $\mathfrak{F}_B\subsetneq\mathfrak{F}$
- *un-coupled* (UC), or fully-decoupled, if $\mathfrak{F}_B=\mathfrak{F}$ (or, equivalently, $\mathfrak{F}_A\subseteq\mathfrak{F}_B$)

In a fully coupled GOFP the control force depends completely upon the implemented control moment, in fact $\mathbf{f}^B=\mathbf{0}$ and thus $\mathbf{f}=\mathbf{f}^A$. In a partially coupled GOFP the projection of the control force onto $\mathfrak{F}_B$ can be chosen freely while the projection onto $\mathfrak{F}_B^{\perp}\cap\mathfrak{F}$ depends completely upon the implemented control moment. Finally in a un-coupled (equivalently, fully decoupled) GOFP no projection of the control force depends on the control moment, i.e., the control force can be freely assigned in the whole space $\mathfrak{F}$. Notice that the full decoupling does not imply necessarily that the control force can be chosen in the whole $\mathbb{R}^3$, unless it holds also $\mathfrak{F}=\mathbb{R}^3$.

The second important classification is provided in the following definition.

Definition 2. A GOFP

- has a *decoupled direction* (D1) if $\dim\mathfrak{F}_B\geq 1$
- has a *decoupled plane* (D2) if $\dim\mathfrak{F}_B\geq 2$
- is *fully actuated* (D3) if $\dim\mathfrak{F}_B=3$.

Combining the previous definitions we say that a GOFP

- has a *single decoupled direction* (SD1) if $\dim\mathfrak{F}_B=1$
- has a *single decoupled plane* (SD2) if $\dim\mathfrak{F}_B=2$.

If a GOFP has a decoupled direction then there exists at least a direction along which the projection of the control force can be chosen freely from the control moment. If a GOFP has a decoupled plane then there exists at least a plane over which the projection of the control force can be chosen freely from the control moment. If a GOFP is fully actuated then the control force can be chosen in all $\mathbb{R}^3$ freely from the control moment.

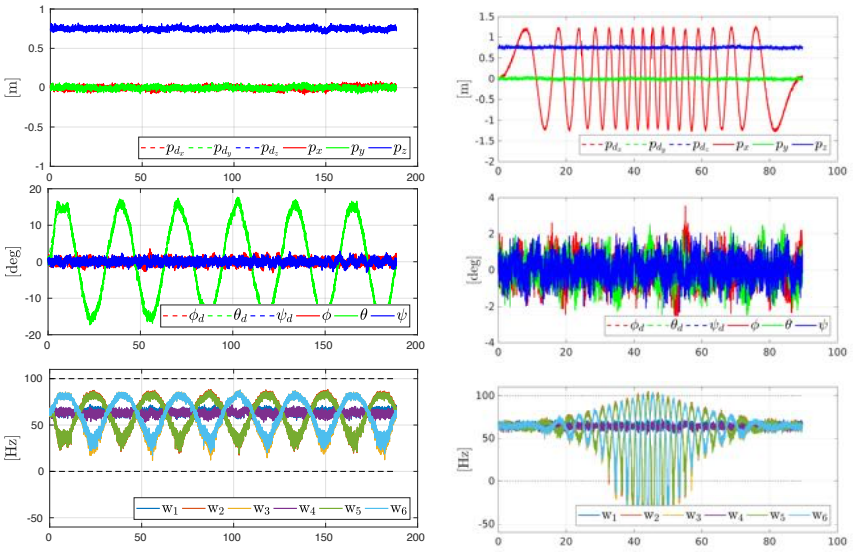

Fig. 42 Two realistic simulations (noise and model uncertainty included) of the TiltHex in Fig. 41 controlled via the inverse dynamics approach. Left column: the TiltHex by LAAS-CNRS follows a trajectory in which the position is constant and the roll varies sinusoidally. Right column: the TiltHex by LAAS-CNRS follows a trajectory in which the orientation is constant and the position follows a chirp signal. Both trajectories are unfeasible for the standard hexarotor in Fig. 40.

In terms of relations between the above definitions, we note that: D3 implies UC, while the converse is not true; D3 implies D2; D2 implies D1. Finally, D1 (and thus D2) can coexist with PC or UC but not with FC. Note that in the state-of-the-art multirotor controllers it is implicitly assumed that the GOFP is fully decoupled and there exists a decoupled direction oriented along its $\mathbf{z}_B$ axis. Nevertheless, in the controller proposed in [184] the decoupled direction can be any and the GOFP can be also partially coupled. Table 9 yields a comprehensive view of all aforementioned definitions and relations. For more examples and insights about GOFP's, as well as for a study of their ability to statically hover after propeller losses we refer the reader to [185].

5 Inverse Dynamics Control for Fully-Actuated Vehicles

Plugging (41) in (40), we obtain

$$\mathbf{a} = \mathbf{M}_R{}^{-1}(\mathbf{b}_R + \mathbf{G}_R\mathbf{G}\mathbf{u}). \tag{49}$$

According to Definition 2 the allocation matrix $\mathbf{G}$ is full-rank for a fully-actuated aerial vehicle, therefore one can choose the following inverse dynamics control law:

$$\mathbf{u} = \mathbf{G}^{\dagger}\mathbf{G}_R{}^{-1}\left(\mathbf{M}_R\mathbf{v} - \mathbf{b}_R\right), \tag{50}$$

which brings the system (49) in the following linear and decoupled form:

$$\mathbf{a} = \mathbf{v}, \tag{51}$$

where $\mathbf{v}$ is a six-dimensional virtual input which can be assigned at will in order to independently steer the six degrees of freedom of the platform along any trajectory, and to ensure robustness of the control scheme. Such classical nonlinear control scheme has been proposed in [237] for fully-actuated aerial vehicles. Figure 42 shows two realistic simulations of the TiltHex executing two trajectories that are unfeasible for a standard collinear hexarotor using the inverse dynamics approach.

The main limitation of the inverse dynamics approach is that, as it is, it does not take into account the input saturations. This fact can easily destabilize the platform when unfeasible inputs are needed in order to perfectly track a given trajectory. This fact can be seen in the simulation of Fig. 43, where the same reference trajectory of Fig. 42-right is used but for the introduction of input limits. In order to overcome this drawback, a more clever controller should be used, as the one that is presented in Chapter 3.6.

6 Conclusions

In this Chapter we have briefly presented the multi-directional thrust aerial platforms emerging from a generic orientation of the propeller angular velocity vectors, i.e., GOFP platforms. We have provided the fundamental definitions of multi-directionality and omnidirectionality and a classification based on the decoupling between the total moment and the total force. In Chapter 3.6 of this book it will be shown how such platforms can be effectively used for aerial physical interaction. One of the most interesting properties of GOFP platforms is their ability, under certain condition, to gain the property to statically hover after propeller losses. Due to the limited amount of space such topic has not been addressed in this chapter, however the reader can find an extensive description of such property in [185].

7 Acknowledgements

The author would like to thank Markus Ryll, Giulia Michieletto, Marco Tognon, and Davide Bicego for their direct and indirect help in the efforts to the setting up of this Chapter.

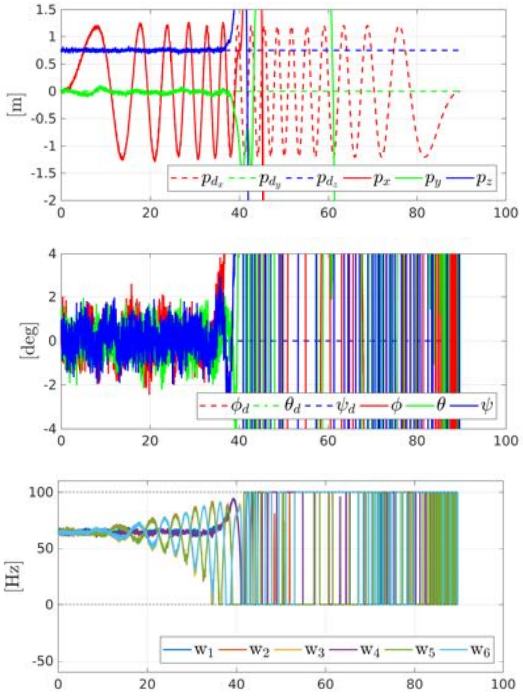

Fig. 43 A realistic simulation (noise and model uncertainty included) of the TiltHex by LAAS-CNRS in Fig. 41 with the addition of input saturation. While tracking the same trajectory of Fig. 42-right the sole inverse dynamics approach makes the system unstable. A controller that overcomes such pitfall is presented in Chapter 3.6.

Chapters in ‘Aerial Robotics Manipulation’, STAR, 2019, Springer

Chapter 3.6
Interaction Control of Platforms with Multi-directional Total Thrust

Antonio Franchi

Abstract The chapter introduces an interaction control framework for multi-directional total thrust platforms. When also fully-actuated, such platforms can modify the total wrench in body frame in any direction. Therefore, they do not suffer from the under-actuation of standard collinear multirotors, and are best suited for dexterous tasks, physical interaction, and for carrying aerial manipulators. The chapter describes in order: a full-pose controller which takes into account the lateral limits of the total force; an algorithm for estimating the contract wrench; and an admittance-shaping framework for physical interaction. Experimental results with the TiltHex platform are also shown to validate the proposed methods.

1 Introduction

Standard multi-rotors (quadrotors, hexarotors, etc.) have collinear propellers generating a total force that is aligned to one direction in body frame, which makes them under-actuated systems. In order to follow a generic position trajectory the total force direction in world frame is changed by rotating the whole vehicle. Maneuvers in which rotation and translation are completely independent are precluded to such platforms, which constitutes a serious problem in the case that, e.g., the platform has to move through a hostile and cluttered ambient or resist a wind gust while keeping a desired attitude. Such an underactuation even deteriorates the potentiality to interact with the environment because it makes impossible to rapidly exert forces in an arbitrarily-chosen direction in the space while keeping a pre-specified orientation.

As described in Chapter 2.3, the main solution to overcome the aforementioned issues has been to mount rotors in a tilted way such that the thrusts of the propellers are not collinear anymore. In this way, the direction of the total force can be changed by selecting the intensity of the force produced by each propeller, without the need of reorienting the whole vehicle. If the propellers are at least six, and the tilting directions do not generate a singular configuration, then direction and intensity of

both the instantaneous total control moment and total control force are, in principle, controllable at will.

However, in order to minimize the waste of energy caused by the appearance of internal forces, the maximum component of the total thrust along the lateral direction is typically kept (by design) much lower than the maximum allowed component along the vertical one. We call these kind of platforms aerial vehicles with *laterally-bounded force* (LBF): they are characterized by a *principal* direction of thrust along which most of the thrust can be exerted. A certain amount of thrust (typically smaller) can be exerted along any non-principal (lateral) directions. This model includes: *i)* the standard underactuated multi-rotor vehicle where thrust is possible *only* along the principal direction, and *ii)* the isotropically fully-actuated platforms where a large amount of total thrust in the lateral directions is applicable [225, 41, 290].

This Chapter is structured as follows. Section 2 presents the generic model of a LBF platforms. Section 3 presents a theoretically grounded 6D tracking control algorithm for LBF platforms is introduced in Sec. 3. Section 4 shows the design of a full architecture to enable 6D interaction control using an admittance control scheme, built around the tracker described in Sec. 3. Results of experiments for the contact-free tracking and interaction control in contact are shown in Sec. 5.1 and 5.2. Finally we conclude the paper and give an outline of further possible extensions in Sec. 6.

2 Model of Laterally-Bounded Force Platforms

In this Section we propose the concept of Laterally-Bounded Force (LBF) Platform, which represents a good approximation of any multi-directional total thrust platform. An LBF platform is a rigid body to which gravity and control generalized forces are applied. All the main symbols are summarized in Table 15 and Fig. 112. Some of the symbols have been already defined at the beginning of the book and are repeated here in order to ease the reading. For the sake of reducing the heaviness of notation, the use of the subscript $\star_b$ is implied in the position, rotation matrix and angular velocity notations. We consider here flying platforms which do not carry any manipulator. Therefore, without risk of confusion, within this Chapter we can denote with $\mathbf{q}$ the configuration $(\mathbf{p},\mathbf{R})$ of the vehicle rather than the one of the manipulator.

The vehicle orientation kinematics is described by $\dot{\mathbf{R}} = \mathbf{R}[\boldsymbol{\omega}]$, where $[\boldsymbol{\omega}]_\times \in so(3)$ is the skew symmetric matrix associated to $\boldsymbol{\omega}$. The control inputs $\mathbf{u}_1 = [u_1\ u_2\ u_3]^T \in \mathbb{R}^3$ and $\mathbf{u}_2 = [u_4\ u_5\ u_6]^T \in \mathbb{R}^3$ are the input force and moment applied to the vehicle expressed in $\mathscr{F}_B$. The following constraint applies

$$[u_1\ u_2]^T \in \mathscr{U}_{xy} \subset \mathbb{R}^2, \tag{142}$$

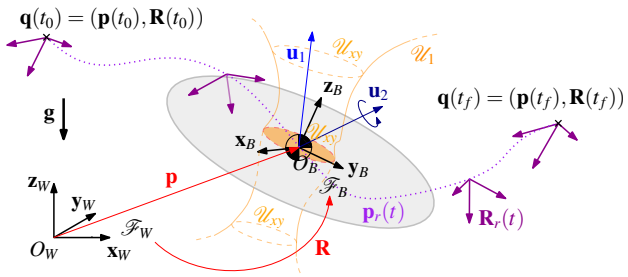

Fig. 112 A drawing illustrating the main quantities of an LBF Aerial Vehicle, the main frames involved, the laterally bounded input sets and the full-pose 6D reference trajectory.

Table 15 Symbols use to define the LBF platform model.

Definition	**Symbol**
World Inertial Frame: $\mathscr{F}_W = O_W, \{\mathbf{x}_W, \mathbf{y}_W, \mathbf{z}_W\}$	$\mathscr{F}_W$
Attached Body Frame: $\mathscr{F}_B = O_B, \{\mathbf{x}_B, \mathbf{y}_B, \mathbf{z}_B\}$	$\mathscr{F}_B$
Position of O_B in $\mathscr{F}_W$, coincident with the Center of Mass (CoM)	$\mathbf{p}_b = \mathbf{p}$
Rotation matrix mapping coordinates in $\mathscr{F}_B$ to coordinates in $\mathscr{F}_W$	$\mathbf{R}_b = \mathbf{R}$
Configuration of the vehicle	$\mathbf{q} = (\mathbf{p}, \mathbf{R})$
Angular velocity of $\mathscr{F}_B$ w.r.t $\mathscr{F}_W$ expr. in $\mathscr{F}_B$	$\boldsymbol{\omega}_b = \boldsymbol{\omega}$
Vehicle's Inertia matrix w.r.t to O_B expressed in $\mathscr{F}_B$	$\mathbf{I}_b$
Control force applied at the CoM expressed in $\mathscr{F}_B$	$\mathbf{u}_1$
Control moment applied at the CoM expressed in $\mathscr{F}_B$	$\mathbf{u}_2$
Feasible set of the control force $\mathbf{u}_1$	$\mathscr{U}_1$
Feasible set of the projection of $\mathbf{u}_1$ on the xy plane in $\mathscr{F}_B$	$\mathscr{U}_{xy}$
i-th vector of the canonical basis of $\mathbb{R}_3$ with $i = 1,2,3$	$\mathbf{e}_i$

where the *laterally bounding* set $\mathscr{U}_{xy}$ is a set that contains the origin. We define $\mathscr{U}_1 = \{\mathbf{u}_1 \in \mathbb{R}^3 \mid [u_1\ u_2]^T \in \mathscr{U}_{xy}, u_3 \geq 0\}$. Note that $\mathscr{U}_{xy}$ can be constant or even be changing depending of u_3, as shown in Figure 112. The dynamics of the aerial platform is then

$$m\ddot{\mathbf{p}} = -mg\mathbf{e}_3 + \mathbf{R}\mathbf{u}_1, \qquad \mathbf{I}_b\dot{\boldsymbol{\omega}} = -\boldsymbol{\omega} \times \mathbf{I}_b\boldsymbol{\omega} + \mathbf{u}_2. \tag{143}$$

Some particularly relevant cases of LBF follow.

Case 1 (Underactuated aerial vehicle) When $\mathscr{U}_{xy} = \{\mathbf{0}\}$ the total force is always oriented as $\mathbf{R}\mathbf{e}_3$ and model (143) becomes the standard underactuated quadrotor model.

Case 2: (Conic LBF) When $\mathscr{U}_{xy} = \{[u_1\ u_2]^T \in \mathbb{R}^2 \mid u_1^2 + u_2^2 \leq (\tan\alpha)^2 u_3^2\}$, model (143) approximates the case of hexarotors with tilted propellers [237, 254], for which the set of allowable $\mathscr{U}_1$ forces has the pseudo-inverted-pyramidal shape. The quantity α is a parameter that represents the tilting angle of the propellers (hexarotor).

Case 3: (Cylindric LBF) When

$$\mathscr{U}_{xy} = \{[u_1\ u_2]^T \in \mathbb{R}^2 \mid u_1^2 + u_2^2 \leq r_{xy}^2\}, \tag{144}$$

Table 16 Symbols related to the LBF platform tracking control.

Definition	Symbol
Reference position for $\mathbf{p}$ at time t	$\mathbf{p}_r(t)$
Reference rotation matrix for $\mathbf{R}$ at time t	$\mathbf{R}_r(t)$
Reference control force to be applied at O_B	$\mathbf{f}_r(t)$ at time t
Set of orientations in $SO(3)$ that allow the application of $\mathbf{f}_r(t)$	$\mathscr{R}(\mathbf{f}_r)$
Subset of $\mathscr{R}(\mathbf{f}_r)$ that minimizes a certain cost w.r.t. $\mathbf{R}_r$	$\overline{\mathscr{R}}(\mathbf{f}_r, \mathbf{R}_r)$
Desired rotation matrix in $\overline{\mathscr{R}}(\mathbf{f}_r, \mathbf{R}_r)$	$\mathbf{R}_d$

model (143) approximates the case of an multirotor with n_m main propellers pointing up and n_s secondary less powerful propellers tilted 90 degrees w.r.t. the main ones, like the one presented in [244], for which the set of allowable $\mathscr{U}_1$ forces can be approximated by a pseudo-cylindric shape

3 Full-pose Tracking Control for LBF Platforms

An underactuated LBF platform (the Case 1 depicted before) is not able to track a generic full-pose trajectory, i.e., with independent position $\mathbf{p}$ and orientation $\mathbf{R}$ in $SE(3)$. The rotation about any axis that is orthogonal to $\mathbf{z}_B$ must follow the evolution over time of $\mathbf{p}$, according to the well-known differential flatness property [188, 79]. Only the tracking og a 4D-pose trajectory (i.e., position $\mathbf{p}$ plus the rotation about $\mathbf{z}_B$) is possible. On the contrary, a 'fully-actuated' LBF platform can exert some force in the lateral direction thus allowing the tracking of a generic full-pose (6D) trajectory. However, due to the bounded thrust along the lateral directions, it is not possible to track *any* full-pose trajectory. The larger the bounds the higher the ability of the platform to track any trajectory, the lower the bounds the more the platform resembles an underactuated multi-rotor and thus it becomes almost unable to track a full-pose trajectory but only a 4D-pose one.

The most straighforward approach to control fully-actuated platforms is the inverse dynamics approach. First, a *control wrench* is computed in order to track the desired trajectory by cancelling the nonlinear dynamical effects and trying to zero the position and orientation errors. Then the thrust inputs for each propeller are computed from the control wrench by simply inverting the control allocation matrix. This method has been first proposed in [237] and then used also in [41] (with pseudo-inversion, in place of inversion, to allocate the input redundancy) and in [225]. The limitation of this control approach is to neglect input saturation, which may easily lead to an unstable behavior if, e.g., the full-pose trajectory to be followed is not input-feasible.

In this Section we briefly present a geometric tracking controller for time-varying references, introduced in [87], that is instead very general and applicable to any LBF vehicle, thus also taking into account the bounds on the lateral control force. The

method is not prone to local orientation representation singularities since it is natively designed in $SE(3)$. The proposed controller ensures, in nominal conditions, the tracking of a full-6D pose reference trajectory (position plus orientation). If the reference orientation and the force needed to track the position trajectory do not comply with the platform constraints, the proposed strategy gives priority to the tracking of the positional part while also tracking the feasible orientation that is the closest to the reference one. This choice is supported by, e.g., the fact that in typical applications a wrong position tracking is more likely to lead to an obstacle crash than a non-perfect orientation tracking. The proposed method also suitable to control vectored-thrust vehicles that can transit from an under-actuated to a fully-actuated configuration while flying – as, e.g., the one presented in [254]. The proposed method is in this sense 'universal', since it does *not* need any switching between two different controllers for each configuration.

Let be given a full-pose trajectory $\mathbf{q}_r(t) = (\mathbf{p}_r(t), \mathbf{R}_r(t)) : [t_0, t_f] \to SE(3)$, where $\mathbf{p}_r(t) \in \mathbb{R}^3$ is the reference position trajectory and $\mathbf{R}_r(t) \in SO(3)$ is the reference attitude trajectory (see Table 16 for a recap of the symbols used in this Section). Inverting (143), the nominal inputs to track $\mathbf{q}_r(t)$ are obtained as $\mathbf{u}_1^r = \mathbf{R}_r^T\,(mg\mathbf{e}_3 + m\ddot{\mathbf{p}}_r)$ and $\mathbf{u}_2^r = \boldsymbol{\omega}_r \times \mathbf{I}_b\boldsymbol{\omega}_r + \mathbf{I}_b\dot{\boldsymbol{\omega}}_r$, where $\boldsymbol{\omega}_r$ is defined by $[\boldsymbol{\omega}_r]_\times = \mathbf{R}_r^T\dot{\mathbf{R}}_r$.

Definition 4 $\mathbf{q}_r(t)$ *is* feasible *if* $\mathbf{u}_1^r(t) \in \mathscr{U}_1\ \forall t \in [t_0, t_f]$.

Exact full-pose (6D) tracking is possible only if $\mathbf{q}_r(t)$ is feasible. However in real world it is not granted that $\mathbf{q}_r(t)$ will be such for the particular LBF platform in use. For this reason, we propose a controller that works (in the sense that the tracking of $\mathbf{p}_r(t)$ is still guaranteed and no singularity appears) even if $\mathbf{q}_r(t)$ is not feasible. Consider the position error $\mathbf{e}_p = \mathbf{p} - \mathbf{p}_r$, velocity error $\mathbf{e}_v = \dot{\mathbf{p}} - \dot{\mathbf{p}}_r$, and two positive definite gain matrices $\mathbf{K}_p$ and $\mathbf{K}_v$. Then consider $\mathbf{f}_r = m\ddot{\mathbf{p}}_r + mg\mathbf{e}_3 - \mathbf{K}_p\mathbf{e}_p - \mathbf{K}_v\mathbf{e}_v$, representing the reference total control force that ideally one would like to apply to the aerial vehicle CoM if the system would be completely fully actuated, i.e., if $\mathscr{U}_1 = \mathbb{R}^3$.

The set of orientations that allow to apply $\mathbf{f}_r$ to the CoM of the LBF aerial vehicle is defined as $\mathscr{R}(\mathbf{f}_r) = \{\mathbf{R} \in SO(3) \mid \mathbf{R}^T\mathbf{f}_r \in \mathscr{U}_1\}$. For an underactuated collinear multi-rotor system the set $\mathscr{R}(\mathbf{f}_r)$ is formed by any $\mathbf{R}$ such that $\mathbf{R}\mathbf{e}_3$ and $\mathbf{f}_r$ are parallel, i.e., $\mathbf{R}\mathbf{e}_3 \times \mathbf{f}_r = 0$. For a generic LBF aerial vehicle the set $\mathscr{R}(\mathbf{f}_r)$ may contain also $\mathbf{R}$'s for which $\mathbf{R}\mathbf{e}_3 \times \mathbf{f}_r \neq 0$. It is possible to show that (see [87] for its proof):

Proposition 2 *The set* $\mathscr{R}(\mathbf{f}_r)$ *is always nonempty* $\forall\ \mathbf{f}_r \in \mathbb{R}^3$.

The proposed controller exploits a cascaded structure[3] by choosing, at each time t, a desired orientation $\mathbf{R}_d \in SO(3)$ that belongs to $\mathscr{R}(\mathbf{f}_r)$ and also minimizes a given cost function w.r.t. $\mathbf{R}_r$. Then one can use the fully actuated rotational dynamics to track $\mathbf{R}_d$ and, in turn, track the reference position $\mathbf{p}_r$. If $\mathbf{q}_r$ is feasible then $\mathbf{R}_d$ will exponentially converge to $\mathbf{R}_r$. Otherwise, only the best feasible orientation will be obtained. Therefore the controller implicitly prioritizes the position trajectory tracking against the orientation one.

[3] Notice that even if a cascaded structure is used, there is no time-scale separation assumption in the proposed controller.

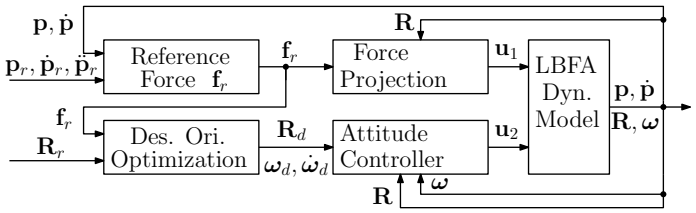

Fig. 113 Block diagram of the 6D tracker for LBF platforms.

Define $\overline{\mathscr{R}}(\mathbf{f}_r, \mathbf{R}_r) \subset \mathscr{R}(\mathbf{f}_r)$ as the set of rotation matrices that solve

$$\min_{\mathbf{R}' \in \mathscr{R}(\mathbf{f}_r)} J(\mathbf{R}_r, \mathbf{R}'),$$

where $J : SO(3) \times SO(3) \to \mathbb{R}_{\geq 0}$ is an arbitraily chosen cost function that represents the degree of similarity between $\mathbf{R}_r$ and $\mathbf{R}'$ one is interested in. The elements in $\overline{\mathscr{R}}(\mathbf{f}_r, \mathbf{R}_r)$ represent orientations of the LBF that allow to apply $\mathbf{f}_r$ and minimize the function J w.r.t. $\mathbf{R}_r$.

Consider that, at each time t a desired orientation $\mathbf{R}_d \in \overline{\mathscr{R}}(\mathbf{f}_r, \mathbf{R}_r)$ is chosen. Furthermore, whenever $\mathbf{R}_r \in \overline{\mathscr{R}}(\mathbf{f}_r, \mathbf{R}_r)$ then $\mathbf{R}_d$ must be chosen equal to $\mathbf{R}_r$. Then define the rotation error $\mathbf{e}_R = \frac{1}{2}(\mathbf{R}_d^T \mathbf{R} - \mathbf{R}^T \mathbf{R}_d)^\vee$, and the angular velocity error $\mathbf{e}_\omega = \boldsymbol{\omega} - \mathbf{R}^T \mathbf{R}_d \boldsymbol{\omega}_d$ where $\bullet^\vee$ is the inverse map of $[\star]_\times$, and $\boldsymbol{\omega}_d$ is the angular velocity associated to $\mathbf{R}_d$. Consider then the following control law

$$\mathbf{u}_1 = \mathrm{sat}_{\mathscr{U}_{xy}}\left((\mathbf{f}_r^T \mathbf{R}\mathbf{e}_1)\mathbf{e}_1 + (\mathbf{f}_r^T \mathbf{R}\mathbf{e}_2)\mathbf{e}_2\right) + (\mathbf{f}_r^T \mathbf{R}\mathbf{e}_3)\mathbf{e}_3 \tag{145}$$

$$\mathbf{u}_2 = \boldsymbol{\omega} \times \mathbf{I}_b \boldsymbol{\omega} - \mathbf{K}_R \mathbf{e}_R - \mathbf{K}_\omega \mathbf{e}_\omega - \mathbf{I}_b\left([\boldsymbol{\omega}]_\times \mathbf{R}^T \mathbf{R}_d \boldsymbol{\omega}_d - \mathbf{R}^T \mathbf{R}_d \dot{\boldsymbol{\omega}}_d\right) \tag{146}$$

where $\mathrm{sat}_{\mathscr{U}_{xy}}(\mathbf{x})$ is a vector in $\mathscr{U}_{xy}$ with the same direction of $\mathbf{x}$, that minimizes the distance from $\mathbf{x}$. $\mathbf{K}_R = k_R \mathbf{I}$ and $\mathbf{K}_\omega = k_\omega \mathbf{I}$ are the gain matrices with $k_R > 0$ and $k_\omega > 0$.

In order to state the convergence properties of the proposed controller let us consider the following error function between two rotation matrixes $\mathbf{R}_1$ and $\mathbf{R}_2$ to be $d(\mathbf{R}_1, \mathbf{R}_2) = \frac{1}{2}\mathrm{tr}\left(\mathbf{I} - \mathbf{R}_2^T \mathbf{R}_1\right)$. the following result holds (see [87] for the proof):

Theorem 1 *Assume that $\mathbf{R}_d(t) \in \mathscr{R}(\mathbf{f}_r(t))$ for any t and that $\boldsymbol{\omega}_d(t)$ and $\dot{\boldsymbol{\omega}}_d(t)$ are well defined for any t. Consider the control $\mathbf{u}_1$ and $\mathbf{u}_2$ defined at (145) and (146).*

Assume that the initial condition satisfies

$$d\left(\mathbf{R}(0), \mathbf{R}_d(0)\right) < 2, \tag{147}$$

$$\|\mathbf{e}_\omega(0)\|^2 < \frac{2}{\lambda_{\min}(\mathbf{I}_b)} k_R \left(1 - d\left(\mathbf{R}(0), \mathbf{R}_d(0)\right)\right) \tag{148}$$

Then, the zero equilibrium of the tracking errors $\mathbf{e}_R$, $\mathbf{e}_\omega$, $\mathbf{e}_p$ and $\mathbf{e}_v$ is exponentially stable. The region of attraction is characterized by (147) and (148).

A block diagram that shows the main subsystems of the proposed control architecture is provided in Fig. 113.

Theorem 1 ensures, under mild conditions, the exponential stability of $\mathbf{e}_p$, $\mathbf{e}_v$, $\mathbf{e}_R$, and $\mathbf{e}_\omega$. Notice that this results holds regardless of the feasibility of $\mathbf{q}_r$. If $\mathbf{q}_r$ is also feasible then exponential tracking of $\mathbf{q}_r$ by $\mathbf{q}$ is also guaranteed. In order to formally state this fact let us define the errors $\mathbf{e}_{R_r} = \frac{1}{2}(\mathbf{R}_r^T\mathbf{R}_d - \mathbf{R}_d^T\mathbf{R}_r)^\vee$, and $\mathbf{e}_{\omega_r} = \boldsymbol{\omega}_d - \mathbf{R}_d\mathbf{R}_r^T\boldsymbol{\omega}_r$.

In next result we characterize the convergence of the above errors to zero provided that the reference trajectory $\mathbf{q}_r(t)$ is *feasible* and satisfies the additional property that $\mathbf{u}_1^r$ is *sufficiently inside* $\mathscr{U}_1$, meaning that there exists a time instant $\bar{t}$ and a positive number ε such that the distance of $\mathbf{u}_1^r$ from the boundary of $\mathscr{U}_1$ is greater than $\varepsilon > 0$ for all $t > \bar{t}$, i,e,

$$\operatorname{dist}(\mathbf{u}_1^r(t), \partial\mathscr{U}_1) > \varepsilon, \qquad \forall t > \bar{t}. \tag{149}$$

Corollary 1 *Assume $\mathbf{q}_r(t)$ is a feasible trajectory and that it satisfies the additional property in (149). Assume that $\mathbf{R}_d(t) \in \mathscr{R}(\mathbf{f}_r(t))$ for any t and that $\boldsymbol{\omega}_d(t)$ and $\dot{\boldsymbol{\omega}}_d(t)$ are well defined for any t. Consider the control $\mathbf{u}_1$ and $\mathbf{u}_2$ defined at (145) and (146). Assume that the initial condition satisfies (147) and (148). Then the zero equilibrium of the tracking errors $\mathbf{e}_R$, $\mathbf{e}_\omega$, $\mathbf{e}_p$ and $\mathbf{e}_v$ is exponentially stable and there exists a time instant $\bar{t} \geq t_0$ such that $\mathbf{e}_{R_r}(t) = \mathbf{e}_{\omega_r}(t) = 0$ for all $t > \bar{t}$. The region of attraction is characterized by (147) and (148).*

The proposed controller (in particular the attitude controller (146)) relies on the availability of $\boldsymbol{\omega}_d$, and $\dot{\boldsymbol{\omega}}_d$. These quantities depend in turn on $\mathbf{R}_d$ which is the output of an optimization algorithm executed at each control step. In order for $\boldsymbol{\omega}_d$ and $\dot{\boldsymbol{\omega}}_d$ to be well defined and available the optimization must ensure a sufficient smoothness of $\mathbf{R}_d$. This could be enforced by adding, e.g., a regularization term in the cost function J. If in the real case at hand this is not possible (or not implementable), then at each time instant in which $\mathbf{R}_d$ is not smooth the attitude controller will undergo a new transient phase. In practice, see the experiments in Sec. 5.1, we have experimentally ascertain that the presence of a few isolated non-smooth instants does not constitute at all a real problem for the stability of the implementation and that regularization is actually not needed for practical stabilization.

The proposed control method is kept on purpose general regarding two main features: the choice of $\mathscr{U}_{xy}$ in (142) and the choice of the cost function J. The former allows the method to be used for a large set of aerial vehicles with different actuation capabilities. The latter allows the engineer to customize the definition of similarity between two orientations in order to comply with the particular task at hand. it is An illustration of how these two general features are particularized for a specific meaningful case is provided in [87].

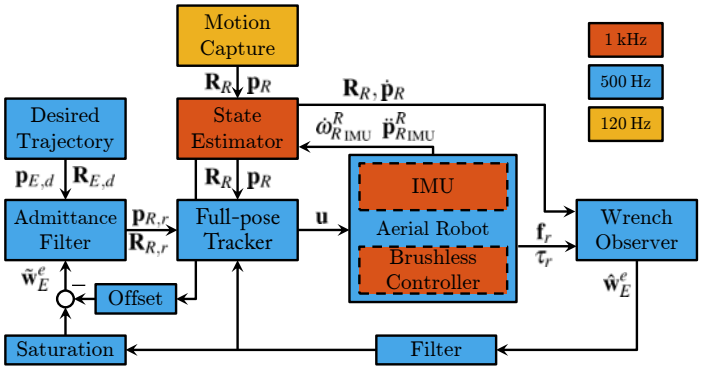

Fig. 114 Signal block diagram of the control framework. The runtime frequency is highlighted. For clarity higher derivatives of the signals have been omitted. The cascaded structure of the pose controller has been omitted as well.

4 Control of the Interaction

In this Section we illustrate how the 6D full-pose tracking controller introduced in Sec. 3 can be integrated in a larger architecture in order to allow the control of the physical interaction with multi-directional thrust platforms.

The control framework is based on an outer loop admittance control and an inner loop full-pose tracking controller (see Fig. 114). The state of the aerial robot is estimated by a Unscented Kalman Filter (UKF) that fuses the Inertial Measurement Unit (IMU) acceleration and angular velocity measurements with the position and orientation from a pose sensor (e.g., a motion capture system or an onboard camera using a Perspective-n-Point (PnP) algorithm). The interaction torques and forces are estimated by a wrench observer. We will now introduce all single components, except for the full-pose tracking controller, already introduced in Sec. 3.

4.1 Contact Wrench Estimation

In order to properly handle physical interaction of the aerial robot with the external environment, the knowledge of the contact interaction wrench between the tool tip and the environment, $\mathbf{w}_E = [\mathbf{f}_E^{\mathrm{T}} \ \boldsymbol{\tau}_E^{\mathrm{T}}]^{\mathrm{T}} \in \mathbb{R}^6$ is essential. To this aim, a force/torque sensor could be mounted on the robot's tool-tip, which is usually capable to provide a reliable measure, but this solution increases both the cost and the weight of the robot. In the aerial robotics field, a more viable solution is the adoption of a wrench estimator, that can provide a sufficiently accurate estimation, denoted as $\hat{\mathbf{w}}_E = [\hat{\mathbf{f}}_E^{\mathrm{T}} \ \hat{\boldsymbol{\tau}}_E^{\mathrm{T}}]^{\mathrm{T}} \in \mathbb{R}^6$, in the presence of accurate measurements of position, velocities and, if available, accelerations.

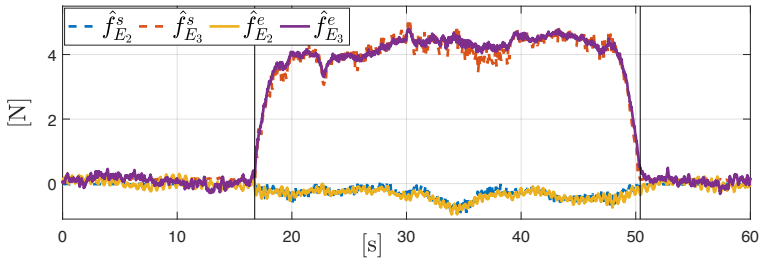

Fig. 115 Estimated versus measured contact force. The ground truth is measured with an ATI45 force torque transducer. The aerial robot pushed the sensor vertically. Both signals have been filtered with a low-pass with a 6 Hz cut-off frequency. For reasons of clarity only the second and third components are presented as the first and second component are overlapping each other a lot.

The external wrench on the robot, $\mathbf{w}_R = [\mathbf{f}_R^{\mathrm{T}}, \ \mathbf{R}_R \tau_R^{R\mathrm{T}}]^{\mathrm{T}}$, can be viewed as the effect on the robot CoM of the wrench $\mathbf{w}_E$ exerted by the environment on the tool tip, namely

$$\mathbf{w}_R = \mathbf{H}_E^{\mathrm{T}}(\mathbf{R}_R)\mathbf{w}_E, \quad \mathbf{H}_E(\mathbf{R}_R) = \begin{bmatrix} \mathbf{I}_3 & -[\mathbf{R}_R \mathbf{p}_E^R]_\times \\ \mathbf{O}_3 & \mathbf{I}_3 \end{bmatrix}. \tag{150}$$

If the sensor equipment provides accurate enough measurements of the platform position and velocities, both angular and linear, while only the linear acceleration, provided by the IMU, can be reasonably used in a wrench observer. Thus we propose the hybrid approach already proposed in [293]. More in detail, the acceleration based observer proposed by [316] is adopted in order to estimate the external interaction forces on the robot CoM, $\mathbf{f}_R$, while the external torques, τ_R^R are obtained by exploiting a momentum-based observer ([63]).

Estimation of contact forces. The following disturbance observer, firstly proposed for aerial robots in [316], is adopted for estimating the contact forces

$$\dot{\hat{\mathbf{f}}}_R = \mathbf{L}(\mathbf{f}_R - \hat{\mathbf{f}}_R) = -\mathbf{L}\hat{\mathbf{f}}_R - \mathbf{L}(m\ddot{\mathbf{p}}_R + mg\mathbf{e}_3 - \mathbf{R}_R\mathbf{F}_1\mathbf{u}), \tag{151}$$

where $\mathbf{L} \in \mathbb{R}^{3\times 3}$ is a gain matrix to be designed. By defining the observer error as $\mathbf{e}_f = \mathbf{f}_R - \hat{\mathbf{f}}_R$, the error dynamics, in the presence of a constant or slowly varying external force is given by [316]

$$\dot{\mathbf{e}}_f + \mathbf{L}\mathbf{e}_f = \mathbf{0}. \tag{152}$$

Thus, the error dynamics is asymptotically convergent to the origin for any positive definite matrix $\mathbf{L}$.

Estimation of contact moments. With reference to the system dynamics (143), the angular momentum $\mathbf{q}^R \in \mathbb{R}^3$ in frame $\mathscr{F}_R$ can be computed as

$$\mathbf{q}^R = \mathbf{J}\omega_R. \tag{153}$$

The time-derivative of (153) can be expressed as

$$\dot{\mathbf{q}}^R = \mathbf{J}\dot{\boldsymbol{\omega}}_R = -\boldsymbol{\omega}_R \times \mathbf{J}\boldsymbol{\omega}_R + \mathbf{F}_2\mathbf{u} + \boldsymbol{\tau}_R^R. \tag{154}$$

By exploiting (154), the estimate $\hat{\boldsymbol{\tau}}_R$ can be seen as the residual vector

$$\hat{\boldsymbol{\tau}}_R^R = \mathbf{K}_I\left[(\mathbf{q}^R(t) - \mathbf{q}^R(t_0)) + \int_{t_0}^{t}(\boldsymbol{\omega}_R \times \mathbf{J}\boldsymbol{\omega}_R - \mathbf{F}_2\mathbf{u} - \hat{\boldsymbol{\tau}}_R^R)\mathrm{d}\tau\right], \tag{155}$$

where t and t_0 are the current and initial time instant respectively, $\mathbf{K}_I$ is a positive definite gain matrix. By reasonably assuming that $\boldsymbol{\omega}_R(t_0) = \mathbf{0_3}$, it implies that $\mathbf{q}^R(t_0)$ is null as well. By taking the time derivative of (155), through (154), the following dynamics for the residual vector is obtained

$$\dot{\hat{\boldsymbol{\tau}}}_R^R + \mathbf{K}_I\hat{\boldsymbol{\tau}}_R^R = \mathbf{K}_I\boldsymbol{\tau}_R^R. \tag{156}$$

Equation (156) is a first order low-pass dynamic system: it can be easily recognized that $\hat{\boldsymbol{\tau}}_R^R \to \boldsymbol{\tau}_R^R$ when $t \to \infty$ and with $\mathbf{K}_I \simeq \infty$. Thus, by properly choosing the matrix $\mathbf{K}_I$, it is possible to achieve a good estimation of $\boldsymbol{\tau}_R^R$ while, at the same time, a low pass filtering of the high-frequency noise.

Estimation of the wrench acting on the tool tip. Once both $\hat{\mathbf{f}}_R$ and $\hat{\boldsymbol{\tau}}_R^R$ are known, the estimated wrench acting on the tool tip, $\hat{\mathbf{w}}_E$ is computed as

$$\hat{\mathbf{w}}_E = \mathbf{H}_E^{-\mathrm{T}}\begin{bmatrix}\hat{\mathbf{f}}_R \\ \mathbf{R}_R\hat{\boldsymbol{\tau}}_R^R\end{bmatrix}. \tag{157}$$

An illustrative example of the wrench observer's precision is presented in Fig. 115. For the sake of clarity, the figure reports only the second and third component of $\hat{\mathbf{w}}_E$ in (157) (continuous lines) against data of an ATI45 force-torque sensor (dotted lines). As for the first component, it shows a behaviour similar to the second one.

4.2 Admittance Filter

In order to achieve bounded forces exchanged with the environment, a compliant behavior could be enforced between the position and orientation of the end-effector and the interaction generalized forces.

Assigned a planned desired trajectory of the end-effector in terms of position $\mathbf{p}_{E,d}$, orientation $\mathbf{R}_{E,d}$, velocities $\boldsymbol{\nu}_{E,d} = [\dot{\mathbf{p}}_{E,d}^{\mathrm{T}} \;\; \mathbf{R}_{E,d}\boldsymbol{\omega}_{E,d}^{\mathrm{T}}]^{\mathrm{T}}$, and accelerations $\dot{\boldsymbol{\nu}}_{E,d}$, the corresponding set of reference motion variables to be fed to the motion controller, $(\mathbf{p}_{E,r}, \mathbf{R}_{E,r}, \boldsymbol{\nu}_{E,r}, \dot{\boldsymbol{\nu}}_{E,r})$, can be generated via an admittance filter, characterized by the following dynamics

$$\mathbf{M}_E\Delta\dot{\boldsymbol{\nu}}_E + \mathbf{D}_E\Delta\boldsymbol{\nu}_E + \mathbf{K}_E\mathbf{e}_E = \hat{\mathbf{w}}_E, \tag{158}$$

where $\Delta\boldsymbol{\nu}_E = \boldsymbol{\nu}_{E,d} - \boldsymbol{\nu}_{E,r}$ is the velocity error, while $\mathbf{e}_E$ is the pose error given by

$$\mathbf{e}_E = \begin{bmatrix} (\mathbf{p}_{E,d} - \mathbf{p}_{E,r})^\top & \left(\frac{1}{2}(\mathbf{R}_{E,d}\mathbf{R}_{E,r}^\mathrm{T} - \mathbf{R}_{E,r}\mathbf{R}_{E,d}^\mathrm{T})^\vee\right)^\top \end{bmatrix}. \tag{159}$$

The (158) represents the dynamics of a 6-DoF mechanical impedance ([271]) of inertia $\mathbf{M}_E$, damping $\mathbf{D}_E$ and stiffness $\mathbf{K}_E$: those matrices are all positive-definite and suitably chosen in a way to impose an over-damped behavior to the system.

Once the reference trajectory of the end-effector has been computed it should be expressed in terms of CoM reference trajectory in order to be tracked by the inner loop pose controller. The reference position and orientation of the robot are then computed as

$$\begin{cases} \mathbf{p}_{R,r} = \mathbf{p}_{E,r} - \mathbf{R}_{R,r}\mathbf{p}_E^R, \\ \mathbf{R}_{R,r} = \mathbf{R}_{E,r}\mathbf{R}_R^E, \end{cases} \tag{160}$$

while the CoM reference velocities and accelerations are obtained by taking the time derivatives of (160). In detail, the reference velocities are given by

$$\begin{cases} \dot{\mathbf{p}}_{R,r} = \dot{\mathbf{p}}_{E,r} - \mathbf{R}_R[\boldsymbol{\omega}_{R,r}]_\times \mathbf{p}_E^R, \\ \boldsymbol{\omega}_{R,r} = \boldsymbol{\omega}_{E,r}, \end{cases} \tag{161}$$

while the reference accelerations are

$$\begin{cases} \ddot{\mathbf{p}}_{R,r} = \ddot{\mathbf{p}}_{E,r} - \mathbf{R}_R[\dot{\boldsymbol{\omega}}_{R,r}]_\times \mathbf{p}_E^R - \mathbf{R}_R[\boldsymbol{\omega}_{R,r}]_\times^2 \mathbf{p}_E^R, \\ \dot{\boldsymbol{\omega}}_{R,r} = \dot{\boldsymbol{\omega}}_{E,r}. \end{cases}$$

5 Experimental Results

5.1 Full-pose Tracking

In Fig. 116 we report the results of an experiment in which the LBF platform shown in Fig. 117 is tasked to track pseudo-sinusoidal trajectory while keeping the orientation horizontal. Thanks to the use of the controller described in Sec. 3, the task is fulfilled as long as the required lateral force is within the bound. When the required force exceeds the bounds the tracking of the orientation is relaxed, however the position tracking is still executed properly. More results and details are provided in [87].

5.2 Interaction Control

In Fig. 118 we report some results of an experiment of interaction control where the platform shown in Fig. 119 is tasked to slide on an inclined surface. The plots

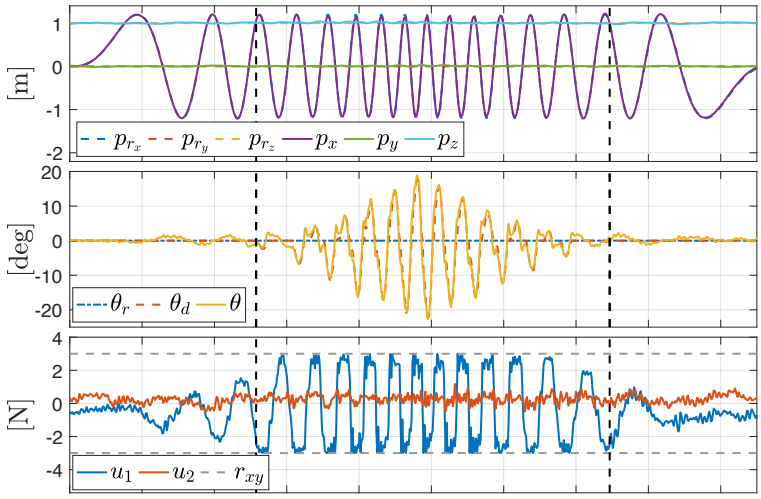

Fig. 116 Exp. 1.1: Desired position: sinusoidal motion along the $\mathbf{x}_W$ axis with constant amplitude and triangular (first increasing then decreasing) frequency. Desired orientation: constantly horizontal. Lateral force bound: constant $r_{xy} = 3\,\mathrm{N}$.

Fig. 117 LAAS-CNRS TiltHex platform used for the tracking experiments.

clearly show how the interaction is stable and interaction forces kept within standard values.

6 Conclusions

In this Chapter we have presented a framework to allow platforms with multi-directional thrust capabilities to perform physical interaction. The method is build around a full-pose tracker, a wrench estimator, an admittance filter and an aerial platform that can accurately execute the total force and moment commands, and measure the real exerted force thanks to the precise control and measurement of the rotational speed of the propellers. It is worth to mention that such platforms and

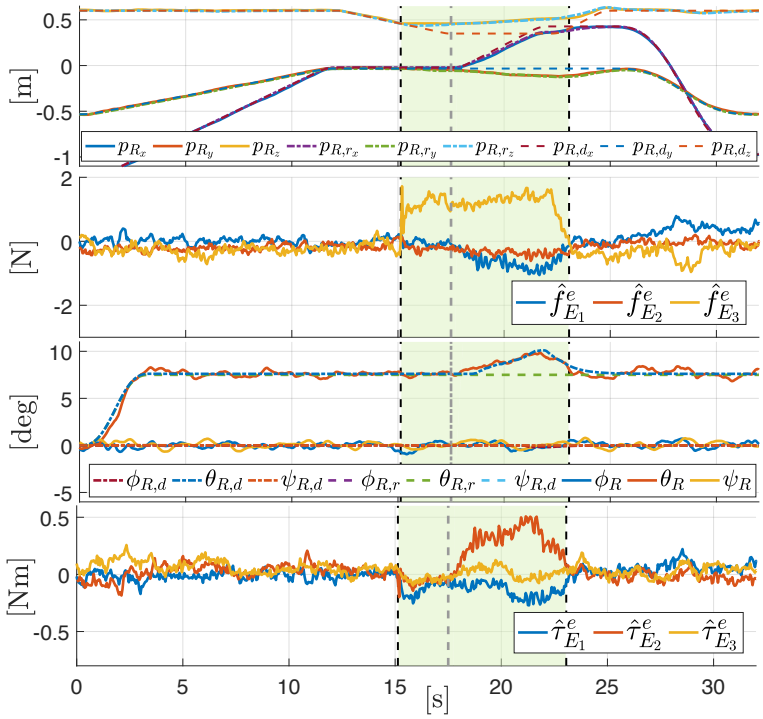

Fig. 118 Sliding with the tool-tip on a tilted surface. The contact phase is highlighted in green, while the actual sliding starts at the gray dashed line: 1) Desired, reference and actual position of the tool-tip. 2) Estimated tool-tip contact forces - low pass filtered (157). 3) Desired, reference and actual tool-tip orientation. 4) Estimated tool-tip contact torques - low pass filtered output of (157).

framework can be used not only in physical interaction with rigid tool but also for aerial manipulation, as recently demonstrated for example in [280].

7 Acknowledgements

The author would like to thank Markus Ryll, Ruggero Carli, Marco Tognon, Davide Bicego, and Francesco Pierri, among others, for their direct and indirect help in the efforts to the setting up of this Chapter.

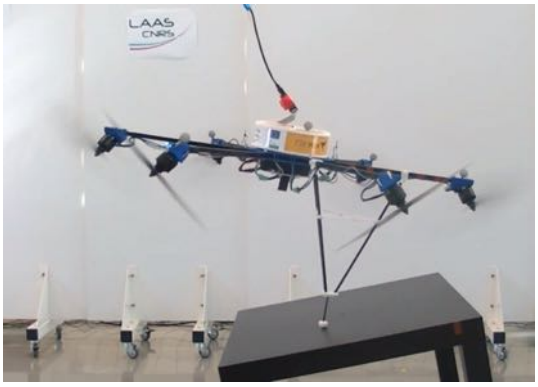

Fig. 119 LAAS-CNRS TiltHex platform used with a rigid tool for physical interaction experiments.

References

1. Aerial Robotics Cooperative Assembly System. In http://www.arcas-project.eu, 20/10/2013.
2. LSD-SLAM: Large-Scale Direct monocular SLAM. 8690 LNCS(PART 2):834–849, 2014.
3. Arcas 4th year experiments. In https://youtu.be/CslR9ArrgBA, 2/1/2016.
4. F. Moreno-Noguer A. Sanfeliu A. Amor-Martinez, A. Ruiz. On-board real-time pose estimation for uavs using deformable visual contour registration. In *2014 IEEE ICRA*, pages 2595–2601, May 2014.
5. R. Adler. *The Geometry of Random Fields*. Society for Industrial and Applied Mathematics, 2010.
6. Rachid Alami, Thierry Simeon, and Jean-Paul Laumond. A geometrical approach to planning manipulation tasks. the case of discrete placements and grasps. In *The fifth international symposium on Robotics research*, pages 453–463. MIT Press, 1990.
7. Alin Albu-Schäffer, Christian Ott, and Gerd Hirzinger. A unified passivity-based control framework for position, torque and impedance control of flexible joint robots. *The International Journal of Robotics Research*, 26(1):23–39, 2007.
8. G. Antonelli. Stability analysis for prioritized closed-loop inverse kinematic algorithms for redundant robotic systems. *IEEE Transactions on Robotics*, 25(5):985–994, October 2009.
9. G. Antonelli, F. Arrichiello, and S. Chiaverini. Experimental kinematic comparison of behavioral approaches for mobile robots. In *16th IFAC World Congress*, Praha, CZ, July 2005.
10. G. Antonelli, F. Arrichiello, and S. Chiaverini. The NSB control: a behavior-based approach for multi-robot systems. *Paladyn Journal of Behavioral Robotics*, 1(1):48–56, 2010.
11. G. Antonelli, F. Arrichiello, and S. Chiaverini. The Null-Space-based Behavioral control for autonomous robotic systems. *Journal of Intelligent Service Robotics*, 1(1):27–39, online March 2007, printed January 2008.
12. G. Antonelli, K. Baizid, F. Caccavale, G. Giglio, and F. Pierri. CAVIS: a control software architecture for cooperative multi-unmanned aerial vehicle-manipulator systems. In *19th World Congress The Int. Federation of Automatic Control*, pages 1108–1113, 2014.
13. R.C. Arkin. Motor schema based mobile robot navigation. *The International Journal of Robotics Research*, 8(4):92–112, 1989.
14. G. Arleo, F. Caccavale, G. Muscio, and F. Pierri. Control of quadrotor aerial vehicles equipped with a robotic arm. In *21st Mediterranean Conference on Control and Automation*, pages 1174–1180, 2013.
15. F. Augugliaro, S. Lupashin, M. Hamer, C. Male, M. Hehn, M. W. Mueller, J. S. Willmann, F. Gramazio, M. Kohler, and R. D'Andrea. The flight assembled architecture installation: Cooperative construction with flying machines. *IEEE Control Systems Magazine*, 34(4):46–64, 2014.
16. P. Baerlocher and R. Boulic. Task-priority formulations for the kinematic control of highly redundant articulated structures. In *IEEE/RSJ International Conference on Intelligent Robots and Systems.*, volume 1, pages 323–329 vol.1, Oct 1998.
17. T. Baier-Lowenstein and Jianwei Zhang. Learning to grasp everyday objects using reinforcement-learning with automatic value cut-off. In *Proc. of IEEE/RSJ IROS*, pages 1551–1556, Oct 2007.
18. K. Baizid, G. Giglio, F. Pierri, M. Trujillo, G. Antonelli, F. Caccavale, A. Viguria, S. Chiaverini, and A. Ollero. Behavioral control of unmanned aerial vehicle manipulator systems. *Autonomous Robots*, 35(8):1–18, 2016.
19. K. Baizid, G. Giglio, F. Pierri, M.A. Trujillo, G. Antonelli, F. Caccavale, A. Viguria, S. Chiaverini, and A. Ollero. Experiments on behavioral coordinated control of an unmanned aerial vehicle manipulator system. In *2015 IEEE International Conference on Robotics and Automation (ICRA)*, pages 4680–4685, Seattle, W, 2015. IEEE.
20. K Baizid, G Giglio, F Pierri, MA Trujillo, G Antonelli, F Caccavale, A Viguria, S Chiaverini, and A Ollero. Behavioral control of unmanned aerial vehicle manipulator systems. *Autonomous Robots*, 41(5):1203–1220, 2017.

21. K. Baizid, G. Giglio, F. Pierri, M.A. Trujillo Soto, G. Antonelli, F. Caccavale, A. Viguria, S. Chiaverini, and A. Ollero. Behavioral control of unmanned aerial vehicle manipulator systems. *Autonomous Robots*, 41(5):1203–1220, online 2016, printed 2017.
22. T. Bartelds, A. Capra, S. Hamaza, S. Stramigioli, and M. Fumagalli. Compliant Aerial Manipulators: Toward a New Generation of Aerial Robotic Workers. *IEEE Robotics and Automation Letters*, 2016.
23. C. D. Bellicoso, L. R. Buonocore, V. Lippiello, and B. Siciliano. Design, modeling and control of a 5-dof light-weight robot arm for aerial manipulation. In *2015 23rd Mediterranean Conference on Control and Automation (MED)*, pages 853–858, June 2015.
24. M. Bernard, K. Kondak, I. Maza, and A. Ollero. Autonomous transportation and deployment with aerial robots for search and rescue missions. *Journal of Field Robotics*, 28(6):914–931, 2011.
25. Markus Bernard and Konstantin Kondak. Generic slung load transportation system using small size helicopters. In *ICRA*, pages 3258–3264. IEEE, 2009.
26. D. P. Bertsekas. *Dynamic Programming and Optimal Control*, volume I. Athena Scientific, 2005.
27. Joshua Bialkowski, Michael Otte, Sertac Karaman, and Emilio Frazzoli. Efficient collision checking in sampling-based motion planning via safety certificates. *The International Journal of Robotics Research*, 35(7):767–796, jun 2016.
28. Georg Biegelbauer, Markus Vincze, and Walter Wohlkinger. Model-based 3d object detection. *Machine Vision and Applications*, 21(4):497–516, 2010.
29. C. M. Bishop. *Pattern recognition and machine learning*. Springer, 2006.
30. M. Björkman, Y. Bekiroglu, V. Högman, and D. Kragic. Enhancing visual perception of shape through tactile glances. In *Proc. of IEEE/RSJ IROS*, pages 3180–3186, Nov 2013.
31. M. Blösch, S. Weiss, D. Scaramuzza, and R. Siegwart. Vision based mav navigation in unknown and unstructured environments. In *2010 IEEE International Conference on Robotics and Automation*, pages 21–28, May 2010.
32. Robert Bodor, Bennett Jackson, and Nikolaos Papanikolopoulos. Vision-based human tracking and activity recognition. In *Proc. of the 11th Mediterranean Conf. on Control and Automation*, volume 1.
33. A. Boeuf. Kinodynamic motion planning for quadrotor-like aerial robots. *PhD Toulouse University*, 2017.
34. A. Boeuf, J. Cortés, R. Alami, and T. Siméon. Planning agile motions for quadrotors in constrained environments. In *Proc. IEEE/RSJ IROS*, 2014.
35. A. Boeuf, J. Cortés, R. Alami, and T. Siméon. Enhancing sampling-based kinodynamic motion planning for quadrotors. In *Proc. IEEE/RSJ IROS*, 2015.
36. C. Borst, M. Fischer, and G. Hirzinger. A fast and robust grasp planner for arbitrary 3d objects. In *Proceedings 1999 IEEE International Conference on Robotics and Automation (Cat. No.99CH36288C)*, volume 3, pages 1890–1896 vol.3, 1999.
37. P. M. Bouffard and S. L. Waslander. A hybrid randomized/nonlinear programming technique for small aerial vehicle trajectory planning in 3d. In *Planning, Perception and Navigation for Intelligent Vehicles (PPNIV) 63, 2009*, 2009.
38. Odile Bourquardez, Robert Mahony, Nicolas Guenard, Franois Chaumette, Tarek Hamel, and Laurent Eck. Image-based visual servo control of the translation kinematics of a quadrotor aerial vehicle. *IEEE Transactions on Robotics*, 25(3):743–749, 2009.
39. A.S. Brandao, J.P.A. Barbosa, V. Mendoza, M. Sarcinelli-Filho, and R. Carelli. A multi-layer control scheme for a centralized uav formation. In *Int. Conf. on Unmanned Aircraft Systems (ICUAS)*, pages 1181–1187, 2014.
40. Leo Breiman. Random forests. *ML*, 45(1):5–32, 2001.
41. D. Brescianini and R. D'Andrea. Design, modeling and control of an omni-directional aerial vehicle. In *2016 IEEE Int. Conf. on Robotics and Automation*, pages 3261–3266, Stockholm, Sweden, May 2016.
42. G. D. Hager C.-P. Lu and E. Mjolsness. Fast and globally convergent pose estimation from video images. *IEEE Transactions on Pattern Analysis and Machine Intelligence*, 22(6):610622, 2000.

43. A. Caballero, M. Bejar, A. Rodriguez-Castaño, and A. Ollero. Motion planning for long reach manipulation in aerial robotic systems with two arms. In *2017 European Conference on Mobile Robots (ECMR)*, pages 1–7, 2017.
44. A. Caballero, M. Bejar, A. Rodriguez-Castaño, and A. Ollero. Motion planning with dynamics awareness for long reach manipulation in aerial robotic systems with two arms. *International Journal of Advanced Robotic Systems*, 15(3), 2018.
45. F. Caccavale, G. Giglio, G. Muscio, and F. Pierri. Adaptive control for uavs equipped with a robotic arm. *IFAC Proceedings Volumes*, 47(3):11049 – 11054, 2014. 19th IFAC World Congress.
46. Fabrizio Caccavale and Masaru Uchiyama. *Cooperative Manipulation*, pages 989–1006. Springer International Publishing, Cham, 2016.
47. Stéphane Cambon, Rachid Alami, and Fabien Gravot. A hybrid approach to intricate motion, manipulation and task planning. *I. J. Robotics Res.*, 28(1):104–126, 2009.
48. R. Cano, C. Pérez, F. Pruaño, A. Ollero, and G. Heredia. Mechanical design of a 6-DOF aerial manipulator for assembling bar structures using UAVs. In *2nd RED-UAS 2013 Workshop on Research, Education and Development of Unmanned Aerial Systems*, 2013.
49. Elisabetta Cataldi, Giuseppe Muscio, Miguel Angel Trujillo, Yamnia Rodríguez, Francesco Pierri, Gianluca Antonelli, Fabrizio Caccavale, Antidio Viguria, Stefano Chiaverini, and Aníbal Ollero. Impedance control of an aerial-manipulator: Preliminary results. In *Intelligent Robots and Systems (IROS), 2016 IEEE/RSJ International Conference on*, pages 3848–3853. IEEE, 2016.
50. M. Ceberio, L. Valera, O. Kosheleva, and R. Romero. Model reduction: Why it is possible and how it can potentially help to control swarms of unmanned arial vehicles (uavs). In *Annual Conf. of the North American Fuzzy Information Processing Society (NAFIPS)*, pages 1–6, 2015.
51. Tan Fung Chan and R. V. Dubey. A weighted least-norm solution based scheme for avoiding joint limits for redundant joint manipulators. *IEEE Transactions on Robotics and Automation*, 11(2):286–292, Apr 1995.
52. F. Chaumette and S. Hutchinson. Visual servo control. i. basic approaches. *IEEE Robotics Automation Magazine*, 13(4):82–90, Dec 2006.
53. Francois Chaumette. Potential Problems of Stability and Convergence in Image-Based and Position-Based Visual Servoing. In *The confluence of vision and control*, number 237 in Lecture Notes in Control and Information Sciences, pages 66–78. Springer, 1998.
54. IC Cheeseman and WE Bennett. The effect of ground on a helicopter rotor in forward flight. 1955.
55. S. Chiaverini. Singularity-robust task-priority redundancy resolution for real-time kinematic control of robot manipulators. *IEEE Transactions on Robotics and Automation*, 13(3):398–410, Jun 1997.
56. S. Chiaverini, G. Oriolo, and I. D. Walker. *Springer Handbook of Robotics*, chapter Kinematically Redundant Manipulators, pages 245–268. B. Siciliano, O. Khatib, (Eds.), Springer-Verlag, Heidelberg, D, 2008.
57. J. Chiverton, X. Xie, and M. Mirmehdi. Automatic bootstrapping and tracking of object contours. 21(3):1231–1245.
58. P.I. Corke and S.A. Hutchinson. A new partitioned approach to image-based visual servo control. *IEEE Transactions on Robotics and Automation*, 17(4):507–515, August 2001.
59. John J. Craig. *Introduction to Robotics: Mechanics and Control (4th Edition)*. Pearson, 4 edition, 2018.
60. A. Criminisi, J. Shotton, and E. Konukoglu. Decision forests: A unified framework for classification, regression, density estimation, manifold learning and semi-supervised learning. *FTCGV*, 7(2–3):81–227, 2011.
61. O. Dahl and L. Nielsen. Torque-limited path following by online trajectory time scaling. *IEEE Trans. on Robotics and Automation*, 6(5):554–561, 1990.
62. Navneet Dalal, Bill Triggs, and Cordelia Schmid. Human detection using oriented histograms of flow and appearance. In *Computer Vision ECCV 2006*, Lecture Notes in Computer Science, pages 428–441. Springer, Berlin, Heidelberg.

63. Alessandro De Luca and Raffaella Mattone. Sensorless robot collision detection and hybrid force/motion control. In *Robotics and Automation, 2005. ICRA 2005. Proceedings of the 2005 IEEE International Conference on*, pages 999–1004. IEEE, 2005.
64. Lavindra De Silva, Mamoun Gharbi, Amit Kumar Pandey, and Rachid Alami. A new approach to combined symbolic-geometric backtracking in the context of human–robot interaction. In *IEEE international conference on robotics and automation (ICRA)*, 2014.
65. Lavindra de Silva, Raphaël Lallement, and Rachid Alami. The HATP hierarchical planner: Formalisation and an initial study of its usability and practicality. In *International Conference on Intelligent Robots and Systems*, 2015.
66. Lavindra de Silva, Amit Kumar Pandey, Mamoun Gharbi, and Rachid Alami. Towards combining HTN planning and geometric task planning. *CoRR*, abs/1307.1482, 2013.
67. D. Devaurs, T. Siméon, and J. Cortés. Optimal path planning in complex cost spaces with sampling-based algorithms. *IEEE Transactions on Automation Science and Engineering, 13(2)*, pages 415–424, 2016.
68. Christian Dornhege, Patrick Eyerich, Thomas Keller, Michael Brenner, and Bernhard Nebel. Integrating task and motion planning using semantic attachments. In *Bridging the Gap Between Task and Motion Planning*, 2010.
69. Christian Dornhege, Andreas Hertle, and Bernhard Nebel. Lazy evaluation and subsumption caching for search-based integrated task and motion planning. In *IROS workshop on AI-based robotics*, 2013.
70. J. C Doyle, K. Glover, P. P. Khargonekar, and B. A. Francis. State-space solutions to standard h_2 and h_∞ control problems. *IEEE Transaction on Automatic Control*, 1989.
71. S. Dragiev, M. Toussaint, and M. Gienger. Gaussian process implicit surfaces for shape estimation and grasping. In *Proc. of IEEE/RSJ ICRA*, pages 2845–2850, May 2011.
72. Mohamed Elbanhawi and Milan Simic. Sampling-Based Robot Motion Planning: A Review. *IEEE Access*, 2:56–77, 2014.
73. F. Endres, J. Hess, J. Sturm, D. Cremers, and W. Burgard. 3-D mapping with an RGB-D camera. *TRO*, 30(1):177–187, 2014.
74. J. Engel, T. Schöps, and D. Cremers. LSD-SLAM: Large-scale direct monocular SLAM. In *ECCV*, pages 834–849. Springer, 2014.
75. Esra Erdem, Kadir Haspalamutgil, Can Palaz, Volkan Patoglu, and Tansel Uras. Combining high-level causal reasoning with low-level geometric reasoning and motion planning for robotic manipulation. In *Robotics and Automation (ICRA), International Conference on*. IEEE, 2011.
76. A. Escande, N. Mansard, and P.-B. Wieber. Hierarchical quadratic programming: Fast online humanoid-robot motion generation. *International Journal of Robotics Research*, 33(7):1006–1028, 2014.
77. B. Espiau, F. Chaumette, and P. Rives. A new approach to visual servoing in robotics. *IEEE Transactions on Robotics and Automation*, 8(3):313–326, June 1992.
78. E. Rodola F. Bergamasco, A. Albarelli and A. Torsello. Rune-tag: A high accuracy fiducial marker with strong occlusion resilience. In *Computer Vision and Pattern Recognition (CVPR), 2011 IEEE Conference on*, pages 113–120.
79. M. Faessler, A. Franchi, and D. Scaramuzza. Differential flatness of quadrotor dynamics subject to rotor drag for accurate tracking of high-speed trajectories. *IEEE Robotics and Automation Letters*, 3(2):620–626, 2018.
80. Y. Fan, S. Haiqing, and W. Hong. A vision-based algorithm for landing unmanned aerial vehicles. pages 993–996, 2008.
81. Amir Massoud Farahmand, Azad Shademan, and Martin Jgersand. Global visual-motor estimation for uncalibrated visual servoing. In *IEEE/RSJ International Conference on Intelligent Robots and Systems*, pages 1969–1974, San Diego, USA, October 2007.
82. M. Fiala. ARTag, a fiducial marker system using digital techniques. In *2005 IEEE Computer Society Conference on Computer Vision and Pattern Recognition (CVPR'05)*, volume 2, pages 590–596 vol. 2.
83. M. Fiala. Designing highly reliable fiducial markers. 32(7):1317–1324.

84. J. Fink, N. Michael, S. Kim, and V. Kumar. Planning and control for cooperative manipulation and transportation with aerial robots. In *14th Int. Symp. on Robotics Research*, Lucerne, Switzerland, Sep. 2009.
85. G. Flores, S. Zhou, R. Lozano, and P. Castillo. A vision and gps-based real-time trajectory planning for mav in unknown urban environments. pages 1150–1155, 2013.
86. Christian Forster, Zichao Zhang, Michael Gassner, Manuel Werlberger, and Davide Scaramuzza. SVO: Semidirect Visual Odometry for Monocular and Multicamera Systems. *IEEE Transactions on Robotics*, 33(2):249–265, 2017.
87. A. Franchi, R. Carli, D. Bicego, and M. Ryll. Full-pose tracking control for aerial robotic systems with laterally-bounded input force. *IEEE Trans. on Robotics*, 2018.
88. M. Fumagalli, R. Naldi, A. Macchelli, R. Carloni, S. Stramigioli, and L. Marconi. Modeling and control of a flying robot for contact inspection. In *2012 IEEE/RSJ Int. Conf. on Intelligent Robots and Systems*, pages 3532–3537, Vilamoura, Portugal, Oct 2012.
89. M. Fumagalli, R. Naldi, A. Macchelli, F. Forte, A. Q. L. Keemink, S. Stramigioli, R. Carloni, and L. Marconi. Developing an aerial manipulator prototype: Physical interaction with the environment. *IEEE Robotics Automation Magazine*, 21(3):41–50, Sept 2014.
90. Francesco M.A. Trujillo-E. Cataldi G. Antonelli F. Caccavale A.Viguria S. Chiaverini G. Muscio, F. Pierri and A. Ollero. Coordinated control of aerial robotic manipulators: Theory and experiments. *IEEE Transactions on Control Systems Technology*, 26(4):1406–1413, 2017.
91. Jeremi Gancet, G. Hattenberger, R. Alami, and S. Lacroix. Task planning and control for a multi-uav system: architecture and algorithms. In *Intelligent Robots and Systems, 2005. (IROS 2005). 2005 IEEE/RSJ Int. Conf. on*, pages 1017–1022, Aug 2005.
92. Caelan Reed Garrett, Tomás Lozano-Pérez, and Leslie Pack Kaelbling. FFRob: An efficient heuristic for task and motion planning. In *International Workshop on the Algorithmic Foundations of Robotics (WAFR)*, 2014.
93. S. Garrido, L. Moreno, D. Blanco, and M. L. Munoz. Sensor-based global planning for mobile robot navigation. *Robotica*, 25(2):189199, 2007.
94. S. Garrido-Jurado, R. Muoz-Salinas, F. J. Madrid-Cuevas, and M. J. Marn-Jimnez. Automatic generation and detection of highly reliable fiducial markers under occlusion. 47(6):2280–2292.
95. Roland Geraerts and Mark H Overmars. Creating high-quality paths for motion planning. *The International Journal of Robotics Research*, 26(8):845–863, 2007.
96. M. P. Gerardo-Castro, T. Peynot, F. Ramos, and R. Fitch. Robust multiple-sensing-modality data fusion using gaussian process implicit surfaces. In *Proc. of FUSION*, pages 1–8, July 2014.
97. Malik Ghallab, Dana Nau, and Paolo Traverso. *Automated Planning: Theory and Practice*. Elsevier, 2004.
98. Mamoun Gharbi, Raphaël Lallement, and Rachid Alami. Combining symbolic and geometric planning to synthesize human-aware plans: toward more efficient combined search. In *2015 IEEE/RSJ International Conference on Intelligent Robots and Systems, IROS 2015, Hamburg, Germany, September 28 - October 2, 2015*, pages 6360–6365, 2015.
99. Gerardo Giglio and Francesco Pierri. Selective compliance control for an unmanned aerial vehicle with a robotic arm. In *Control and Automation (MED), 2014 22nd Mediterranean Conference of*, pages 1190–1195. IEEE, 2014.
100. G. Gioioso, A. Franchi, G. Salvietti, S. Scheggi, and D. Prattichizzo. The Flying Hand: a formation of UAVs for cooperative aerial tele-manipulation. In *2014 IEEE Int. Conf. on Robotics and Automation*, pages 4335–4341, Hong Kong, China, May. 2014.
101. G. Gioioso, M. Ryll, D. Prattichizzo, H. H. Bülthoff, and A. Franchi. Turning a near-hovering controlled quadrotor into a 3D force effector. In *2014 IEEE Int. Conf. on Robotics and Automation*, pages 6278–6284, Hong Kong, China, May. 2014.
102. K. Glover and J. C. Doyle. State-space fomulae for all stabilizing controller that satisfy an h_∞ norm bound and realations to risk sensitivity. *Systems and Control Letters*, 1988.

103. C Goerzen, Z Kong, and B Mettler. A Survey of Motion Planning Algorithms from the Perspective of Autonomous UAV Guidance. *Journal of Intelligent and Robotic Systems*, 57(1-4):65–100, jan 2010.
104. S. Gottschlich, C. Ramos, and D. Lyons. Assembly and task planning: a taxonomy. *Robotics Automation Magazine, IEEE*, 1(3):4–12, Sept 1994.
105. Fabien Gravot, Stephane Cambon, and Rachid Alami. aSyMov: a planner that deals with intricate symbolic and geometric problems. In *Robotics Research*, pages 100–110. Springer, 2005.
106. G. Greiner and K. Hormann. Efficient clipping of arbitrary polygons. *ACM Transactions on Graphics (TOG)*, 17(2):71–83, 1998.
107. Michael Gschwandtner, Roland Kwitt, Andreas Uhl, and Wolfgang Pree. BlenSor: Blender Sensor Simulation Toolbox Advances in Visual Computing. volume 6939 of *Lecture Notes in Computer Science*, chapter 20, pages 199–208. Springer Berlin / Heidelberg, Berlin, Heidelberg, 2011.
108. Zhenjun Han, Qixiang Ye, and Jianbin Jiao. Online feature evaluation for object tracking using kalman filter. In *2008 19th International Conference on Pattern Recognition*, pages 1–4.
109. K. Hashimoto, T. Kimoto, T. Ebine, and H. Kimura. Manipulator control with image-based visual servo. In *IEEE International Conference on Robotics and Automation*, pages 2267–2271, Sacramento, USA, April 1991.
110. James S Hayden. The effect of the ground on helicopter hovering power required. In *Proc. AHS 32nd Annual Forum*, 1976.
111. Frederik Heger and Sanjiv Singh. Robust robotic assembly through contingencies, plan repair and re-planning. In *International Conference on Robotics and Automation*, 2010.
112. Markus Hehn and Raffaello D'Andrea. Quadrocopter trajectory generation and control. *IFAC Proceedings Volumes*, 44(1):1485–1491, 2011.
113. G. Heredia, A. E. Jimenez-Cano, I. Sanchez, D. Llorente, V. Vega, J. Braga, J. A. Acosta, and A. Ollero. Control of a multirotor outdoor aerial manipulator. In *IEEE International Conference on Intelligent Robots and Systems*, 2014.
114. Joel A Hesch, Dimitrios G Kottas, Sean L Bowman, and Stergios I Roumeliotis. Camera-imu-based localization: Observability analysis and consistency improvement. *The International Journal of Robotics Research*, 33(1):182–201, 2014.
115. Neville Hogan. Impedance control: An approach to manipulation: Parts i-iii. *Journal of dynamic systems, measurement, and control*, 107(1):1–24, 1985.
116. D. Honegger, L. Meier, P. Tanskanen, and M. Pollefeys. An open source and open hardware embedded metric optical flow cmos camera for indoor and outdoor applications. In *2013 IEEE International Conference on Robotics and Automation*, pages 1736–1741, May 2013.
117. Armin Hornung, Kai M. Wurm, Maren Bennewitz, Cyrill Stachniss, and Wolfram Burgard. OctoMap: An efficient probabilistic 3D mapping framework based on octrees. *Autonomous Robots*, 34(3):189–206, 2013.
118. Koh Hosoda and Minoru Asada. Versatile visual servoing without knowledge of true jacobian. In *IEEE/RSJ International Conference on Intelligent Robots and Systems*, pages 186–193, Munich, Germany, September 1994.
119. F. Huber, K. Kondak, K. Krieger, D. Sommer, M. Schwarzbach, M. Laiacker, I. Kossyk, S. Parusel, S. Haddadin, and A. Albu-Schaffer. First analysis and experiments in aerial manipulation using fully actuated redundant robot arm. In *2013 IEEE/RSJ International Conference on Intelligent Robots and Systems*, pages 3452–3457, Tokyo, J, 2013.
120. S. Hutchinson, G. D. Hager, and P. I. Corke. A tutorial on visual servo control. *IEEE Transactions on Robotics and Automation*, 12(5):651–670, Oct 1996.
121. C. Domokos J. Nemeth and Z. Kato. Recovering planar homographies between 2d shapes. In *Proccedings of ICCV*, pages 113–120.
122. P. K. Jain. Homography estimation from planar contours. In *3D Data Processing, Visualization, and Transmission, Third International Symposium on*, pages 877–884.
123. F. Janabi-Sharifi, L. Deng, and W. J. Wilson. Comparison of basic visual servoing methods. *IEEE/ASME Transactions on Mechatronics*, 16(5):967–983, Oct 2011.

124. P. Jiménez. Survey on assembly sequencing: a combinatorial and geometrical perspective. *Journal of Intelligent Manufacturing*, 24(2):235–250, apr 2013.
125. A. E. Jimenez-Cano, J. Martin, G. Heredia, A. Ollero, and R. Cano. Control of an aerial robot with multi-link arm for assembly tasks. In *2013 ICRA*, pages 4916–4921, May 2013.
126. AE Jimenez-Cano, J Braga, Guillermo Heredia, and Aníbal Ollero. Aerial manipulator for structure inspection by contact from the underside. In *Intelligent Robots and Systems (IROS), 2015 IEEE/RSJ International Conference on*, pages 1879–1884. IEEE, 2015.
127. A.E. Jimenez-Cano, J. Martin, G. Heredia, A. Ollero, and R. Cano. Control of an aerial robot with multi-link arm for assembly tasks. In *IEEE International Conference on Robotics and Automation*, pages 4916–4921, Karlsruhe, D, 2013.
128. Leslie Pack Kaelbling and Tomás Lozano-Pérez. Hierarchical task and motion planning in the now. In *Robotics and Automation (ICRA), International Conference on*, pages 1470–1477. IEEE, 2011.
129. Z. Kalal, J. Matas, and K. Mikolajczyk. P-N learning: Bootstrapping binary classifiers by structural constraints. In *Proc. of the IEEE Conf. on Computer Vision and Pattern Recognition (CVPR)*, pages 49–56, 2010.
130. Lars Karlsson, Julien Bidot, Fabien Lagriffoul, Alessandro Saffiotti, Ulrich Hillenbrand, and Florian Schmidt. Combining task and path planning for a humanoid two-arm robotic system. In *Proceedings of TAMPRA: Combining Task and Motion Planning for Real-World Applications (ICAPS workshop)*, pages 13–20. Citeseer, 2012.
131. H. Kato and M. Billinghurst. Marker tracking and hmd calibration for a video-based augmented reality conferencing system. In *1999.(IWAR99) Proceedings in Augmented Reality*, page 8594, 1999.
132. H. Kato, M. Billinghurst, I. Poupyrev, K. Imamoto, and K. Tachibana. Virtual object manipulation on a table-top AR environment. In *Proceedings IEEE and ACM International Symposium on Augmented Reality (ISAR 2000)*, pages 111–119.
133. L.E. Kavraki, P. Svestka, J.-C. Latombe, and M.H. Overmars. Probabilistic roadmaps for path planning in high-dimensional configuration spaces. *IEEE Transactions on Robotics and Automation*, 12(4):566–580, 1996.
134. Lydia Kavraki, Jean-Claude Latombe, and Randall H. Wilson. On the complexity of assembly partitioning. *Information Processing Letters*, 48(5):229 – 235, 1993.
135. Jonathan Kelly and Gaurav S. Sukhatme. Visual-inertial sensor fusion: Localization, mapping and sensor-to-sensor self-calibration. *International Journal of Robotics Research*, 30(1):56–79, Jan 2011.
136. O. Khatib. A unified approach for motion and force control of robot manipulators: The operational space formulation. *IEEE Journal of Robotics and Automation*, 3(1):43–53, 1987.
137. J. Kim and D.H. Shim. A vision-based target tracking control system of a quadrotor by using a tablet computer. pages 1165–1172, 2013.
138. S. Kim, S. Choi, and H. J. Kim. Aerial manipulation using a quadrotor with a two DOF robotic arm. In *2013 IEEE/RSJ Int. Conf. on Intelligent Robots and Systems*, pages 4990–4995, Nov 2013.
139. Soohwan Kim and Jonghyuk Kim. *GPmap: A Unified Framework for Robotic Mapping Based on Sparse Gaussian Processes*, pages 319–332. Results of the 9th International Conference, Field and Service Robotics. Springer International Publishing, 2015.
140. G. Klein and D. Murray. Parallel tracking and mapping for small AR workspaces. In *ISMAR*, pages 225–234. IEEE, 2007.
141. Georg Klein and David Murray. Parallel tracking and mapping for small AR workspaces. *2007 6th IEEE and ACM International Symposium on Mixed and Augmented Reality, ISMAR*, 2007.
142. Ross A. Knepper, Todd Layton, John Romanishin, and Daniela Rus. Ikeabot: An autonomous multi-robot coordinated furniture assembly system. In *International Conference on Robotics and Automation*, pages 855–862, 2013.
143. Stefan Kohlbrecher, Oskar Von Stryk, Johannes Meyer, and Uwe Klingauf. A flexible and scalable SLAM system with full 3D motion estimation. *9th IEEE International Symposium on Safety, Security, and Rescue Robotics, SSRR 2011*, pages 155–160, 2011.

144. K. Kondak, M. Bernard, N. Meyer, and G. Hommel. Autonomously flying vtol-robots: Modeling and control. In *Proceedings - IEEE International Conference on Robotics and Automation*, pages 736–741, 2007.
145. Konstantin Kondak, Markus Bernard, N. Losse, and Günter Hommel. Elaborated modeling and control for autonomous small size helicopters. In *International ISR/Robotik Joint Conference*, pages 207–208. VDI, 2006.
146. Konstantin Kondak, Markus Bernard, Nicolas Meyer, and Gunter Hommel. Autonomously flying VTOL-robots: Modeling and control. In *Robotics and Automation (ICRA), 2007 IEEE International Conference on*, pages 736–741. IEEE, 2007.
147. Konstantin Kondak, Kai Krieger, Alin Albu-Schäffer, Marc Schwarzbach, Maximilian Laiacker, Ivan Maza, Angel Rodriguez-Castano, and Anibal Ollero. Closed-loop behavior of an autonomous helicopter equipped with a robotic arm for aerial manipulation tasks. IJARS, 2013.
148. Konstantin Kondak, Aníbal Ollero, Ivan Maza, Kai Krieger, Alin Albu-Schaeffer, Marc Schwarzbach, and Maximilian Laiacker. Unmanned aerial systems physically interacting with the environment: Load transportation, deployment, and aerial manipulation. In *Handbook of Unmanned Aerial Vehicles*, pages 2755–2785. Springer Netherlands, 2015.
149. C. Korpela, M. Orsag, T. Danko, B. Kobe, C. McNeil, R. Pisch, and P. Oh. Flight stability in aerial redundant manipulators. In *2012 ICRA*, pages 3529–3530, May 2012.
150. E. Koyuncu and G. Inalhan. A probabilistic b-spline motion planning algorithm for unmanned helicopters flying in dense 3d environments. In *Proc. IEEE/RSJ IROS 2008*, 2008.
151. Fabien Lagriffoul, Dimitar Dimitrov, Alessandro Saffiotti, and Lars Karlsson. Constraint propagation on interval bounds for dealing with geometric backtracking. In *Intelligent Robots and Systems (IROS), RSJ International Conference on*, pages 957–964. IEEE, 2012.
152. Raphaël Lallement, Lavindra de Silva, and Rachid Alami. HATP: An HTN planner for robotics. In *2nd ICAPS Workshop on Planning and Robotics*, pages 20–27, 2014.
153. S. LaValle and J. Kuffner. Rapidly-exploring random trees: progress and prospects. In *Algorithmic and Computational Robotics: New Directions*. A. K. Peters, Wellesley, MA, 2001.
154. S.M. LaValle and J.J. Kuffner. Randomized kinodynamic planning. *International Journal of Robotics Research, 20(5)*, pages 378–400, 2001.
155. Steven LaValle. *Planning Algorithms*. Cambridge University Press, Cambridge, U.K., 2006.
156. Steven M LaValle and James J Kuffner. Randomized kinodynamic planning. *The International Journal of Robotics Research*, 20(5):378–400, 2001.
157. Yann Lecun, Urs Muller, Jan Ben, and Eric Cosatto. Off-Road Obstacle Avoidance through End-to-End Learning.
158. T. Lee, M. Leok, and N. H. McClamroch. Nonlinear robust tracking control of a quadrotor uav on se(3). In *2012 American Control Conference (ACC)*, pages 4649–4654, June 2012.
159. Taekhee Lee and Young J Kim. Massively parallel motion planning algorithms under uncertainty using POMDP. *The International Journal of Robotics Research*, 35(8):928–942, jul 2016.
160. Taeyoung Lee, Melvin Leoky, and N Harris McClamroch. Geometric tracking control of a quadrotor uav on se (3). In *Decision and Control (CDC), 2010 49th IEEE Conference on*, pages 5420–5425. IEEE, 2010.
161. Beatriz "León, Antonio Morales, and Joaquin" Sancho-Bru. *"Robot Grasping Foundations"*, pages "15–31". "Springer International Publishing", "2014".
162. V. Lepetit and P. Fua. Keypoint recognition using randomized trees. *IEEE Transactions on Pattern Analysis and Machine Intelligence*, 28(9):1465–1479, 2006.
163. M. Li and A. I. Mourikis. Improving the accuracy of ekf-based visual-inertial odometry. In *2012 IEEE International Conference on Robotics and Automation*, pages 828–835, May 2012.
164. Mingyang Li and Anastasios I. Mourikis. High-precision, consistent ekf-based visual-inertial odometry. *The International Journal of Robotics Research*, 32(6):690–711, 2013.
165. V. Lippiello and F. Ruggiero. Cartesian impedance control of a uav with a robotic arm. In *10th IFAC Symposium on Robot Control (SYROCO)*, pages 229–234, Sept 2012.

166. Vincenzo Lippiello, Jonathan Cacace, Angel Santamaria-Navarro, Juan Andrade-Cetto, Miguel ngel Trujillo, Yamnia Rodrguez Esteves, and Antidio Viguria. Hybrid visual servoing with hierarchical task composition for aerial manipulation. *IEEE Robotics and Automation Letters*, 1(1):259–266, Jan 2016.
167. Vincenzo Lippiello, Bruno Siciliano, and Luigi Villani. Position-based visual servoing in industrial multirobot cells using a hybrid camera configuration. *IEEE Transactions on Robotics*, 23(1):73–86, February 2007.
168. X. Liu, L. Lin, S. Yan, H. Jin, and W. Jiang. Adaptive object tracking by learning hybrid template online. 21(11):1588–1599.
169. Yi Liu and Y. F. Zheng. Video object segmentation and tracking using psi;-learning classification. 15(7):885–899.
170. Y. Long and D. J. Cappelleri. *Omnicopter: A Novel Overactuated Micro Aerial Vehicle*, pages 215–226. Springer International Publishing, Heidelberg, 2013.
171. Tomás Lozano-Pérez and Leslie Pack Kaelbling. A constraint-based method for solving sequential manipulation planning problems. *IROS*, 2014.
172. B. Lucas and T. Kanade. An iterative image registration technique with an application to stereo vision. In *Proceedings of the 7th IJCAI*.
173. Venkatesh K Madyastha, Vishal C Ravindra, Srinath Mallikarjunan, and Anup Goyal. Extended Kalman filter vs. error state Kalman filter for aircraft attitude estimation. In *AIAA Guidance, Navigation and Control Conference*, pages 6615–6638, Portland, August 2011.
174. R. Mahony, V. Kumar, and P. Corke. Multirotor aerial vehicles: Modeling, estimation, and control of quadrotor. *IEEE Robotics Automation Magazine*, 19(3):20–32, Sept 2012.
175. E. Malis, F. Chaumette, and S. Boudet. 2 frac12;d visual servoing. *IEEE Transactions on Robotics and Automation*, 15(2):238–250, Apr 1999.
176. N. Mansard, O. Khatib, and A. Kheddar. A unified approach to integrate unilateral constraints in the stack of tasks. *Robotics, IEEE Transactions on*, 25(3):670–685, 2009.
177. Nicolas Mansard and François Chaumette. Task sequencing for high-level sensor-based control. *Robotics, IEEE Trans. on*, 23(1):60–72, 2007.
178. W. Martens, Y. Poffet, P. R. Soria, R. Fitch, and S. Sukkarieh. Geometric priors for gaussian process implicit surfaces. *IEEE Robotics and Automation Letters*, 2(2):373–380, April 2017.
179. A. Masselli, S. Yang, K.E. Wenzel, and A. Zell. A cross-platform comparison of visual marker based approaches for autonomous flight of quadrocopters. pages 685–693, 2013.
180. I. Maza, K. Kondak, M. Bernard, and A. Ollero. Multi-UAV cooperation and control for load transportation and deployment. *Journal of Intelligent and Robotic Systems*, 57:417–449, 2010.
181. Ivan Maza, Aníbal Ollero, Enrique Casado, and David Scarlatti. Classification of multi-uav architectures. In *Handbook of Unmanned Aerial Vehicles*. Springer Netherlands, 2015.
182. D. Mellinger and V. Kumar. Minimum snap trajectory generation and control for quadrotors. In *Proc. IEEE ICRA*, 2011.
183. D. Mellinger, Q. Lindsey, M. Shomin, and V. Kumar. Design, modeling, estimation and control for aerial grasping and manipulation. In *IEEE International Conference on Intelligent Robots and Systems*, pages 2668–2673, 2011.
184. G. Michieletto, M. Ryll, and A. Franchi. Control of statically hoverable multi-rotor aerial vehicles and application to rotor-failure robustness for hexarotors. In *2017 IEEE Int. Conf. on Robotics and Automation*, pages 2747–2752, Singapore, May 2017.
185. G. Michieletto, M. Ryll, and A. Franchi. Fundamental actuation properties of multi-rotors: Force-moment decoupling and fail-safe robustness. *IEEE Trans. on Robotics*, 2018.
186. A. T. Miller, S. Knoop, H. I. Christensen, and P. K. Allen. Automatic grasp planning using shape primitives. In *2003 IEEE International Conference on Robotics and Automation (Cat. No.03CH37422)*, volume 2, pages 1824–1829 vol.2, Sept 2003.
187. Andrew T. Miller, Steffen Knoop, Henrik I. Christensen, and Peter K. Allen. Automatic grasp planning using shape primitives. In *Proc. of IEEE ICRA*, 2003.
188. V. Mistler, A. Benallegue, and N. K. M'Sirdi. Exact linearization and noninteracting control of a 4 rotors helicopter via dynamic feedback. In *10th IEEE Int. Symp. on Robots and Human Interactive Communications*, pages 586–593, Bordeaux, Paris, France, Sep. 2001.

189. S. Moe, G. Antonelli, A. Teel, K. Pettersen, and J. Schrimpf. Set-based tasks within the singularity-robust multiple task-priority inverse kinematics framework: General formulation, stability analysis and experimental results. *Frontiers in Robotics and AI*, 3:16, 2016.
190. I.F. Mondragon, P. Campoy, J.F. Correa, and L. Mejias. Visual model feature tracking for uav control. pages 1–6, 2007.
191. F. Moreno-Noguer, V. Lepetit, and P. Fua. Accurate non-iterative O(n) solution to the pnp problem. In *ICCV*, pages 1–8. IEEE, 2007.
192. F. Moreno-Noguer, V. Lepetit, and P. Fua. Pose priors for simultaneously solving alignment and correspondence. In *Proc. of the IEEE Europ. Conf. on Computer Vision (ECCV)*, volume 2, pages 405–418, 2008.
193. H. Mosemann and F.M. Wahl. Automatic decomposition of planned assembly sequences into skill primitives. *Robotics and Automation, IEEE Transactions on*, 17(5):709–718, Oct 2001.
194. M. W. Mueller, M. Hehn, and R. D'Andrea. A computationally efficient algorithm for state-to-state quadrocopter trajectory generation and feasibility verification. In *Proc. IEEE/RSJ IROS*, 2013.
195. Jorge Muñoz-Morera, Francisco Alarcon, Ivan Maza, and Anibal Ollero. Combining a hierarchical task network planner with a constraint satisfaction solver for assembly operations involving routing problems in a multi-robot context. *International Journal of Advanced Robotic Systems*, 15(3):1–13, June 2018.
196. Jorge Muñoz-Morera, Ivan Maza, Fernando Caballero, and Anibal Ollero. Architecture for the automatic generation of plans for multiple UAS from a generic mission description. *Journal of Intelligent & Robotic Systems*, 84(1):493–509, 2016.
197. R. Mur-Artal, J. M. M. Montiel, and J. D. Tardós. ORB-SLAM: a versatile and accurate monocular slam system. *TRO*, 31(5):1147–1163, 2015.
198. Raul Mur-Artal, J. M.M. Montiel, and Juan D. Tardos. ORB-SLAM: A Versatile and Accurate Monocular SLAM System. *IEEE Transactions on Robotics*, 31(5):1147–1163, 2015.
199. G. Muscio, F. Pierri, M. A. Trujillo, E. Cataldi, G. Antonelli, F. Caccavale, A. Viguria, S. Chiaverini, and A. Ollero. Coordinated control of aerial robotic manipulators: Theory and experiments. *IEEE Transactions on Control Systems Technology*, PP(99):1–8, 2017.
200. G. Muscio, F. Pierri, M. A. Trujillo, E. Cataldi, G. Giglio, G. Antonelli, F. Caccavale, A. Viguria, S. Chiaverini, and A. Ollero. Experiments on coordinated motion of aerial robotic manipulators. In *2016 IEEE Int. Conf. on Robotics and Automation*, pages 1224–1229, Stockholm, Sweden, May 2016.
201. G. Muscio, F. Pierri, M.A. Trujillo, E. Cataldi, G. Antonelli, F. Caccavale, A. Viguria, S. Chiaverini, and A. Ollero. Coordinated control of aerial robotic manipulators: theory and experiments. *IEEE Transactions on Control Systems Technology*, 2017.
202. Yoshihiko Nakamura. *Advanced robotics - redundancy and optimization.* Addison-Wesley, 1991.
203. Yoshihiko Nakamura, Hideo Hanafusa, and Tsuneo Yoshikawa. Task-priority based redundancy control of robot manipulators. *The International Journal of Robotics Research*, 6(2):3–15, 1987.
204. Dana Nau, Tsz-Chiu Au, Okhtay Ilghami, Ugur Kuter, J. William Murdock, Dan Wu, and Fusun Yaman. SHOP2: An HTN planning system. *JAIR*, 20(1):379–404, 2003.
205. Dana Nau, Malik Ghallab, and Paolo Traverso. *Automated Planning: Theory & Practice*. Morgan Kaufmann Publishers Inc., San Francisco, CA, USA, 2004.
206. Srinivas Nedunuri, Sailesh Prabhu, Mark Moll, Swarat Chaudhuri, and Lydia E Kavraki. Smt-based synthesis of integrated task and motion plans from plan outlines. In *IEEE international conference on robotics and automation (ICRA)*, 2014.
207. H. Nguyen and D. Lee. Hybrid force/motion control and internal dynamics of quadrotors for tool operation. In *2013 IEEE/RSJ Int. Conf. on Intelligent Robots and Systems*, pages 3458–3464, Tokyo, Japan, Nov. 2013.
208. Matthias Nieuwenhuisen, David Droeschel, Marius Beul, and Sven Behnke. Autonomous navigation for micro aerial vehicles in complex gnss-denied environments. *Journal of Intelligent & Robotic Systems*, 84(1):199–216, Dec 2016.

209. Kenichiro Nonaka and Hirokazu Sugizaki. Integral sliding mode altitude control for a small model helicopter with ground effect compensation. In *American Control Conference (ACC), 2011*, pages 202–207. IEEE, 2011.
210. Stephen Nuske, Sanjiban Choudhury, Sezal Jain, Andrew Chambers, Luke Yoder, Sebastian Scherer, Lyle Chamberlain, Hugh Cover, and Sanjiv Singh. Autonomous Exploration and Motion Planning for an Unmanned Aerial Vehicle Navigating Rivers. *Journal of Field Robotics*, 32(8):1141–1162, dec 2015.
211. A. Ollero. *"Robotica. Manipuladores y robots moviles"*. Marcombo, 2001.
212. E. Olson. AprilTag: A robust and flexible visual fiducial system. In *2011 IEEE International Conference on Robotics and Automation*, pages 3400–3407.
213. Matko Orsag, Christopher Korpela, Stjepan Bogdan, and Paul Oh. Valve turning using a dual-arm aerial manipulator. In *Unmanned Aircraft Systems (ICUAS), 2014 International Conference on*, pages 836–841. IEEE, 2014.
214. Matko Orsag, Christopher Korpela, Paul Oh, and Stjepan Bogdan. *Aerial Manipulator Dynamics*, pages 123–163. Springer International Publishing, Cham, 2018.
215. C. Ott. *Cartesian Impedance Control of Redundant and Flexible-Joint Robots*, volume 49 of *Springer Tracts in Advanced Robotics*. Springer-Verlag, Berlin Heidelberg, D, 2008.
216. C. Ott, A. Albu-Schaffer, A. Kugi, and G. Hirzinger. On the passivity-based impedance control of flexible joint robots. *IEEE Transactions on Robotics*, 24(2):416–429, 2008.
217. C. Ott, A. Dietrich, and A. Albu-Schäffer. Prioritized multi-task compliance control of redundant manipulators. *Automatica*, 53(1):416–423, 2015.
218. Michael Otte and Emilio Frazzoli. RRTX: Asymptotically optimal single-query sampling-based motion planning with quick replanning. *The International Journal of Robotics Research*, 35(7):797–822, jun 2016.
219. M. Ozuysal, M. Calonder, V. Lepetit, and P. Fua. Fast keypoint recognition using random ferns. *IEEE Transactions on Pattern Analysis and Machine Intelligence*, 32(3):448–461, 2010.
220. J. Pan, B. Hu, and J. Q. Zhang. Robust and accurate object tracking under various types of occlusions. 18(2):223–236.
221. Jia Pan and Dinesh Manocha. Fast probabilistic collision checking for sampling-based motion planning using locality-sensitive hashing. *The International Journal of Robotics Research*, 35(12):1477–1496, oct 2016.
222. George Papageorgiou. Two-degree-of-freedom control of an actively controlled wind-tunnel model. *Journal of Guidance, Control, and Dynamics*, 25, July-August 2002.
223. Jeremie Papon, Alexey Abramov, Markus Schoeler, and Florentin Wörgötter. Voxel cloud connectivity segmentation - supervoxels for point clouds. In *Proc. of the 2013 IEEE CVPR*, CVPR '13, pages 2027–2034, Washington, DC, USA, 2013. IEEE Computer Society.
224. C Park, J Pan, and D Manocha. Parallel Motion Planning Using Poisson-Disk Sampling. *IEEE Transactions on Robotics*, 33(2):359–371, 2017.
225. S. Park, Jongbeom J. Her, J. Kim, and D. Lee. Design, modeling and control of omni-directional aerial robot. In *2016 IEEE/RSJ Int. Conf. on Intelligent Robots and Systems*, pages 1570–1575, Daejeon, South Korea, 2016.
226. A. Penate-Sanchez, J. Andrade-Cetto, and F. Moreno-Noguer. Exhaustive linearization for robust camera pose and focal length estimation. *IEEE Transactions on Pattern Analysis and Machine Intelligence*, 35(10):2387–2400, Oct 2013.
227. Jenelle Armstrong Piepmeier, Gary V. McMurray, and Harvey Lipkin. Uncalibrated dynamic visual servoing. *IEEE Transactions on Robotics and Automation*, 20(1):143–147, 2004.
228. Erion Plaku and Gregory D Hager. Sampling-based motion and symbolic action planning with geometric and differential constraints. In *Robotics and Automation (ICRA), International Conference on*, pages 5002–5008. IEEE, 2010.
229. Fatih Porikli and Alper Yilmaz. Object detection and tracking. In *Video Analytics for Business Intelligence*, Studies in Computational Intelligence, pages 3–41. Springer, Berlin, Heidelberg.
230. I Postlethwaite and A. Yue, editors. *Improvement of Helicopter Handling Qualities using H_∞-Optimisation*, 1990.

231. P. E. I. Pounds, D. R. Bersak, and A. M. Dollar. Grasping from the air: Hovering capture and load stability. In *2011 ICRA*, pages 2491–2498, May 2011.
232. Caitlin Powers, Daniel Mellinger, Aleksandr Kushleyev, Bruce Kothmann, and Vijay Kumar. Influence of aerodynamics and proximity effects in quadrotor flight. In *Experimental robotics*, pages 289–302. Springer, 2013.
233. Jerry Pratt, Ben Krupp, and Chris Morse. Series elastic actuators for high fidelity force control. 29:234–241, 06 2002.
234. A. Pumarola, A. Vakhitov, A. Agudo, A. Sanfeliu, and F. Moreno-Noguer. PL-SLAM: Real-Time Monocular Visual SLAM with Points and Lines. In *International Conference in Robotics and Automation*, 2017.
235. M. Quigley, K. Conley, B. Gerkey, J. Faust, T. Foote, J. Leibs, R. Wheeler, and A. Y. Ng. ROS: an open-source robot operating system. In *ICRAW*, volume 3, page 5. Kobe, Japan, 2009.
236. M. Quigley, B. Gerkey, K. Conley, J. Faust, T. Foote, J. Leibs, E. Berger, R. Wheeler, and A. Ng. Ros: an open-source robot operating system. In *Open-source software workshop of the 2009 IEEE International Conference on Robotics and Automation*, Kobe, J, 2009.
237. S. Rajappa, M. Ryll, H. H. Bülthoff, and A. Franchi. Modeling, control and design optimization for a fully-actuated hexarotor aerial vehicle with tilted propellers. In *2015 IEEE Int. Conf. on Robotics and Automation*, pages 4006–4013, Seattle, WA, May 2015.
238. C. E. Rasmussen and C. K. I. Williams. *Gaussian Processes for Machine Learning*. The MIT Press, 2006.
239. Vishal C. Ravindra, Venkatesh K. Madyastha, and Anup Goyal. The equivalence between two well-known variants of the Kalman filter. In *International Conference on Advances in Control and Optimization of Dynamic Systems*, Feb 2012.
240. J. Rekimoto. Matrix: a realtime object identification and registration method for augmented reality. In *Proceedings. 3rd Asia Pacific Computer Human Interaction (Cat. No.98EX110)*, pages 63–68.
241. Andrew C. Rice, Robert K. Harle, and Alastair R. Beresford. Analysing fundamental properties of marker-based vision system designs. 2(4):453–471.
242. C. Richter, A. Bry, and N. Roy. Polynomial trajectory planning for aggressive quadrotor flight in dense indoor environments. In *Proc. ISRR*, 2013.
243. Máximo A. Roa and Raúl Suárez. Grasp quality measures: review and performance. *Autonomous Robots*, 38(1):65–88, 2015.
244. H. Romero, S. Salazar, A. Sanchez, and R. Lozano. A new UAV configuration having eight rotors: dynamical model and real-time control. In *46th IEEE Conf. on Decision and Control*, pages 6418–6423, New Orleans, LA, Dec. 2007.
245. J. Rosell. Assembly and task planning using petri nets: A survey. In *Proceedings of the I MECH E Part B journal of engineering manufacture*, volume 218, pages 987–994, 2004.
246. R. Rossi, A. Santamaria-Navarro, J. Andrade-Cetto, and P. Rocco. Trajectory generation for unmanned aerial manipulators through quadratic programming. *IEEE Robotics and Autom. Letters*, 2(2):389–396, April 2017.
247. Cyril Roussillon, Aurélien Gonzalez, Joan Solà, Jean Marie Codol, Nicolas Mansard, Simon Lacroix, and Michel Devy. RT-SLAM: A generic and real-time visual SLAM implementation. In *Computer Vision Systems*, volume 6962 of *Lect. Notes in Comp. Science*, pages 31–40. Springer Berlin Heidelberg, 2011.
248. Ethan Rublee, Vincent Rabaud, Kurt Konolige, and Gary Bradski. Orb: An efficient alternative to sift or surf. In *Computer Vision (ICCV), 2011 IEEE international conference on*, pages 2564–2571. IEEE, 2011.
249. M Ruffo, M Di Castro, L Molinari, R Losito, A Masi, J Kovermann, and Luis Rodrigues. New infrared time-of-flight measurement sensor for robotic platforms. In *International Symposium and International Workshop on ADC Modelling and Testing*, pages 13–18, September 2014.
250. F. Ruggiero, J. Cacace, H. Sadeghian, and V. Lippiello. Impedance control of VToL UAVs with a momentum-based external generalized forces estimator. In *2014 IEEE International Conference on Robotics and Automation*, pages 2093–2099, Hong Kong, C, 2014.

251. F. Ruggiero, J. Cacace, H. Sadeghian, and V. Lippiello. Passivity-based control of VToL UAVs with a momentum-based estimator of external wrench and unmodeled dynamics. *Robotics and Autonomous Systems*, 72:139–151, 2015.
252. F. Ruggiero, M.A. Trujillo, R. Cano, H. Ascorbe, A. Viguria, C. Peréz, V. Lippiello, A. Ollero, and B. Siciliano. A multilayer control for multirotor UAVs equipped with a servo robot arm. In *2015 IEEE International Conference on Robotics and Automation*, pages 4014–4020, Seattle, WA, USA, 2015.
253. Fabio Ruggiero, Jonathan Cacace, Hamid Sadeghian, and Vincenzo Lippiello. Passivity-based control of vtol uavs with a momentum-based estimator of external wrench and unmodeled dynamics. *Robotics and Autonomous Systems*, 72:139 – 151, 2015.
254. M. Ryll, D. Bicego, and A. Franchi. Modeling and control of FAST-Hex: a fully-actuated by synchronized-tilting hexarotor. In *2016 IEEE/RSJ Int. Conf. on Intelligent Robots and Systems*, pages 1689–1694, Daejeon, South Korea, Oct. 2016.
255. M. Ryll, H. H. Bülthoff, and P. Robuffo Giordano. A novel overactuated quadrotor unmanned aerial vehicle: modeling, control, and experimental validation. *IEEE Trans. on Control Systems Technology*, 23(2):540–556, 2015.
256. Markus Ryll, Giuseppe Muscio, Francesco Pierri, Elisabetta Cataldi, Gianluca Antonelli, Fabrizio Caccavale, and Antonio Franchi. 6d physical interaction with a fully actuated aerial robot. In *2017 IEEE International Conference on Robotics and Automation*, 2017.
257. PJ Sánchez-Cuevas, G Heredia, and A Ollero. Multirotor uas for bridge inspection by contact using the ceiling effect. In *Unmanned Aircraft Systems (ICUAS), 2017 International Conference on*, pages 767–774. IEEE, 2017.
258. PJ Sanchez-Cuevas, Guillermo Heredia, and Anibal Ollero. Experimental approach to the aerodynamic effects produced in multirotors flying close to obstacles. In *Iberian Robotics conference*, pages 742–752. Springer, 2017.
259. J.L. Sanchez-Lopez, S. Saripalli, P. Campoy, J. Pestana, and C. Fu. Toward visual autonomous ship board landing of a vtol uav. pages 779–788, 2013.
260. D. Santamaria, F. Alarcon, A. Jimenz, A. Viguria, M. Béjar, and A. Ollero. Model-based design, development and validation for UAS critical software. *Journal of Intelligent & Robotic Systems*, 65(1–4):103–114, 2012.
261. A. Santamaria-Navarro, P. Grosch, V. Lippiello, J. Sol, and J. Andrade-Cetto. Uncalibrated visual servo for unmanned aerial manipulation. *IEEE/ASME Transactions on Mechatronics*, 22(4):1610–1621, Aug 2017.
262. A. Santamaria-Navarro, V. Lippiello, and J. Andrade-Cetto. Task priority control for aerial manipulation. In *IEEE International Symposium on Safety, Security, and Rescue Robotics (SSRR)*, pages 1–6, Oct 2014.
263. A. Santamaria-Navarro, J. Solà, and J. Andrade-Cetto. High-frequency mav state estimation using low-cost inertial and optical flow measurement units. In *Intelligent Robots and Systems (IROS), 2015 IEEE/RSJ International Conference on*, pages 1864–1871, Sept 2015.
264. Angel Santamaria-Navarro and Juan Andrade-Cetto. Uncalibrated image-based visual servoing. In *IEEE International Conference on Robotics and Automation*, pages 5247–5252, Karlsruhe, Germany, May 2013.
265. Angel Santamaria-Navarro, Giuseppe Loianno, Joan Solà, Vijay Kumar, and Juan Andrade-Cetto. Autonomous navigation of micro aerial vehicles using high-rate and low-cost sensors. *Autonomous Robots, To appear.*, Dec 2018.
266. Ashutosh Saxena, Justin Driemeyer, and Andrew Y Ng. Robotic grasping of novel objects using vision. *The International Journal of Robotics Research*, 27(2):157–173, 2008.
267. Azad Shademan, Amir-Massoud Farahmand, and Martin Jgersand. Robust jacobian estimation for uncalibrated visual servoing. In *IEEE International Conference on Robotics and Automation*, pages 5564–5569, Anchorage, USA, May 2010.
268. I Sharf, M Nahon, A Harmat, W Khan, M Michini, N Speal, M Trentini, T Tsadok, and T Wang. Ground effect experiments and model validation with draganflyer x8 rotorcraft. In *Unmanned Aircraft Systems (ICUAS), 2014 International Conference on*, pages 1158–1166. IEEE, 2014.

269. J. Shotton, M. Johnson, and R. Cipolla. Semantic texton forests for image categorization and segmentation. In *Proc. of the IEEE Conf. on Computer Vision and Pattern Recognition (CVPR)*, pages 1–8, 2008.
270. B. Siciliano, L. Sciavicco, L. Villani, and G. Oriolo. *Robotics: modelling, planning and control*. Springer Verlag, 2009.
271. B. Siciliano, L. Sciavicco, L. Villani, and G. Oriolo. *Robotics: Modelling, Planning and Control*. Springer, 2009.
272. Sanni Siltanen, Mika Hakkarainen, and Petri Honkamaa. Automatic marker field calibration. In *Proc. Virtual Reality International Conference (VRIC2007), Laval, France*, pages 261–267.
273. Thierry Siméon, Jean-Paul Laumond, and Florent Lamiraux. Move3D: a generic platform for path planning. In *Proc. IEEE ISATP*, 2001.
274. E. Simetti, G. Casalino, S. Torelli, A. Sperindé, and A. Turetta. Floating underwater manipulation: Developed control methodology and experimental validation within the TRIDENT project. *Journal of Field Robotics*, 31(3):364–385, 2013.
275. S. Simi, R. Kurup, and S. Rao. Distributed task allocation and coordination scheme for a multi-uav sensor network. In *10th Int. Conf. on Wireless and Optical Communications Networks*, pages 1–5, July 2013.
276. K. Simonyan and A. Zisserman. Very deep convolutional networks for large-scale image recognition. In *in arXiv preprint: 1409*, page 1556, 2014.
277. Sigurd Skogestad and I.Ian Postlethwaite. *Multivariable Feedback Control: Analysis and Design*. Wiley, 2nd edition, 2005.
278. D. Song, K. Huebner, V. Kyrki, and D. Kragic. Learning task constraints for robot grasping using graphical models. In *Proc. of IEEE/RSJ IROS*, 2010.
279. Siddharth Srivastava, Eugene Fang, Lorenzo Riano, Rohan Chitnis, Stuart Russell, and Pieter Abbeel. Combined task and motion planning through an extensible planner-independent interface layer. *IEEE international conference on robotics and automation (ICRA)*, 2014.
280. N. Staub, D. Bicego, Q. Sablé, V. Arellano-Quintana, S. Mishra, and A. Franchi. Towards a flying assistant paradigm: the OTHex. In *2018 IEEE Int. Conf. on Robotics and Automation*, Brisbane, Australia, May 2018.
281. J. Sturm, N. Engelhard, F. Endres, W. Burgard, and D. Cremers. A benchmark for the evaluation of RGB-D SLAM systems. In *IROS*, Oct. 2012.
282. A. Suarez, G. Heredia, and A. Ollero. Lightweight compliant arm for aerial manipulation. In *2015 IEEE/RSJ International Conference on Intelligent Robots and Systems (IROS)*, pages 1627–1632, 2015.
283. A. Suarez, G. Heredia, and A. Ollero. Lightweight compliant arm with compliant finger for aerial manipulation and inspection. In *2016 IEEE/RSJ International Conference on Intelligent Robots and Systems (IROS)*, pages 4449–4454, 2016.
284. A. Suarez, G. Heredia, and A. Ollero. Design of an anthropomorphic, compliant and lightweight dual arm for aerial manipulation. *IEEE Access*, pages 1–1, 2018.
285. A. Suarez, G. Heredia, and A. Ollero. Physical-virtual impedance control in ultralightweight and compliant dual-arm aerial manipulators. *IEEE Robotics and Automation Letters*, 3(3):2553–2560, 2018.
286. Alejandro Suarez, Guillermo Heredia, and Anibal Ollero. Vision-based deflection estimation in an anthropomorphic, compliant and lightweight dual arm. In Anibal Ollero, Alberto Sanfeliu, Luis Montano, Nuno Lau, and Carlos Cardeira, editors, *ROBOT 2017: Third Iberian Robotics Conference*, pages 332–344, Cham, 2018. Springer International Publishing.
287. Alejandro Suarez, Antonio Enrique Jimenez-Cano, Victor Manuel Vega, Guillermo Heredia, Angel Rodriguez-Castao, and Anibal Ollero. Design of a lightweight dual arm system for aerial manipulation. *Mechatronics*, 50:30 – 44, 2018.
288. Ulrike Thomas and Friedrich M. Wahl. Assembly planning and task planning - two prerequisites for automated robot programming. In Daniel Schütz and Friedrich M. Wahl, editors, *Robotic Systems for Handling and Assembly*, volume 67 of *Springer Tracts in Advanced Robotics*, pages 333–354. Springer Berlin Heidelberg, 2011.

289. M. Tognon and A. Franchi. Dynamics, control, and estimation for aerial robots tethered by cables or bars. *IEEE Trans. on Robotics*, 33(4):834–845, 2017.
290. M. Tognon and A. Franchi. Omnidirectional aerial vehicles with unidirectional thrusters: Theory, optimal design, and control. *IEEE Robotics and Automation Letters*, 2018.
291. M. Tognon, A. Testa, E. Rossi, and A. Franchi. Takeoff and landing on slopes via inclined hovering with a tethered aerial robot. In *2016 IEEE/RSJ Int. Conf. on Intelligent Robots and Systems*, pages 1702–1707, Daejeon, South Korea, Oct. 2016.
292. M. Tognon, B. Yüksel, G. Buondonno, and A. Franchi. Dynamic decentralized control for protocentric aerial manipulators. In *2017 IEEE Int. Conf. on Robotics and Automation*, pages 6375–6380, Singapore, May 2017.
293. T. Tomic, C. Ott, and S. Haddadin. External wrench estimation, collision detection, and reflex reaction for flying robots. *IEEE Transactions on Robotics*, PP(99):1–17, 2017.
294. Arturo Torres-González, Jose Ramiro Martinez-de Dios, and Anibal Ollero. Range-only slam for robot-sensor network cooperation. *Autonomous Robots*, 42(3):649–663, Mar 2018.
295. Nikolas Trawny and Stergios I. Roumeliotis. Indirect Kalman filter for 3D attitude estimation. *University of Minnesota, Dept. of Computer Science & Engineering, Technical Report*, 2, rev. 57, 2005.
296. Hideyuki Tsukagoshi, Masahiro Watanabe, Takahiro Hamada, Dameitry Ashlih, and Ryuma Iizuka. Aerial manipulator with perching and door-opening capability. In *Robotics and Automation (ICRA), 2015 IEEE International Conference on*, pages 4663–4668. IEEE, 2015.
297. F. Moreno-Noguer V. Lepetit and P. Fua. Epnp: An accurate o (n) solution to the pnp problem. *International Journal of Computer Vision*, 81(2):155166, 2009.
298. A. Vakhitov, J. Funke, and F. Moreno-Noguer. Accurate and linear time pose estimation from points and lines. In *ECCV*, 2016.
299. K. P. Valavanis. *Advances in Unmanned Aerial Vehicles: State of the Art and the Road to Autonomy*, volume 33 of *Intelligent Systems, Control and Automation: Science and Engineering*. Springer, 2007.
300. Kimon P. Valavanis and George J. Vachtsevanos. *Handbook of Unmanned Aerial Vehicles*. Springer Publishing Company, Incorporated, 2014.
301. VICON. Vicon Motion Systems. Ltd.
302. M. Villamizar, J. Andrade-Cetto, A. Sanfeliu, and F. Moreno-Noguer. Boosted random ferns for object detection. *IEEE Transactions on Pattern Analysis and Machine Intelligence*, 2017.
303. M. Villamizar, A. Garrell, A. Sanfeliu, and F. Moreno-Noguer. Online human-assisted learning using random ferns. In *Proc. International Conference on Pattern Recognition (ICPR)*, pages 2821–2824, 2012.
304. M. Villamizar, A. Sanfeliu, and F. Moreno-Noguer. Fast online learning and detection of natural landmarks for autonomous aerial robots. In *Proc. of the IEEE Int. Conf. on Robotics & Automation (ICRA)*, pages 4996–5003, 2014.
305. R. G. von Gioi, J. Jakubowicz, J. M. Morel, and G. Randall. LSD: a line segment detector. *IPOL*, 2:35–55, 2012.
306. R. Voyles and G. Jiang. A nonparallel hexrotor UAV with faster response to disturbances for precision position keeping. In *2014 IEEE Int. Symp. on Safety, Security and Rescue Robotics*, pages 1–5, West Lafayette, IN, Oct. 2014.
307. Daniel Wagner and Dieter Schmalstieg. Artoolkitplus for pose tracking on mobile devices. In *Proceedings of 12th Computer Vision Winter Workshop (CVWW'07)*, pages 139–146, 2007.
308. D.J. Walker and I. Postlethwaite. Advanced helicopter flight control using two-degree-of-freedom h_∞ optimization. 1996.
309. Stephan Weiss, Davide Scaramuzza, and Roland Siegwart. Monocular-SLAM-based navigation for autonomous micro helicopters in gps denied environments. *Journal of Field Robotics*, 28(6):854–874, 2011.
310. Oliver Williams and Andrew Fitzgibbon. Gaussian process implicit surfaces. In *Gaussian Processes In Practice*, June 2006.
311. W.J. Wilson, C.C. Williams Hulls, and G.S. Bell. Relative end-effector control using Cartesian position based visual servoing. *IEEE Transactions on Robotics and Automation*, 12(5):684–696, October 1996.

312. M. Haddad Y. Bouktir and T. Chettibi. Trajectory planning for a quadrotor helicopter. In *Control and Automation, 2008, 16th Mediterranean Conference on*, 2008.
313. H. Yang and D. Lee. Dynamics and control of quadrotor with robotic manipulator. In *2014 IEEE International Conference on Robotics and Automation (ICRA)*, pages 5544–5549, May 2014.
314. S. Yang, S.A. Scherer, and A. Zell. An onboard monocular vision system for autonomous takeoff, hovering and landing of a micro aerial vehicle. 69(1–4):499–515, 2013.
315. B. Yüksel, C. Secchi, H. H. Bülthoff, and A. Franchi. Aerial physical interaction via reshaping of the physical properties: Passivity-based control methods for nonlinear force observers. In *ICRA 2014 Workshop: Aerial robots physically interacting with the environment*, Hong Kong, China, May. 2014.
316. B. Yüksel, C. Secchi, H. H. Bülthoff, and A. Franchi. A nonlinear force observer for quadrotors and application to physical interactive tasks. In *2014 IEEE/ASME Int. Conf. on Advanced Intelligent Mechatronics*, pages 433–440, Besançon, France, Jul. 2014.
317. B. Yüksel, C. Secchi, H. H. Bülthoff, and A. Franchi. Reshaping the physical properties of a quadrotor through IDA-PBC and its application to aerial physical interaction. In *2014 IEEE Int. Conf. on Robotics and Automation*, pages 6258–6265, Hong Kong, China, May. 2014.
318. B. Yksel, G. Buondonno, and A. Franchi. Differential flatness and control of protocentric aerial manipulators with any number of arms and mixed rigid-/elastic-joints. In *2016 IEEE/RSJ International Conference on Intelligent Robots and Systems (IROS)*, pages 561–566, Oct 2016.
319. B. Yksel, S. Mahboubi, C. Secchi, H. H. Blthoff, and A. Franchi. Design, identification and experimental testing of a light-weight flexible-joint arm for aerial physical interaction. In *2015 IEEE International Conference on Robotics and Automation (ICRA)*, pages 870–876, May 2015.
320. Ji Zhang and Sanjiv Singh. LOAM: Lidar Odometry and Mapping in Real- time. *IEEE Transactions on Robotics*, 32(July):141–148, 2015.
321. X. Zhang, W. Hu, W. Qu, and S. Maybank. Multiple object tracking via species-based particle swarm optimization. 20(11):1590–1602.